(2)

FINAL REPORT

ON

CONTRACT N00014-83-C-0303

SAIC-85/1683

SAIC™

Science Applications International Corporation

Post Office Box 1303, 1710 Goodridge Drive, McLean, Virginia 22102, (703) 821-4300

Final Report

on

Contract N00014-83-C-0303

SAIC-85/1683

April 1985

Prepared

by

C.W. Spofford

SCIENCE APPLICATIONS INTERNATIONAL CORPORATION

1710 Goodridge Drive
P.O. Box 1303
McLean, VA 22102
(703) 821-4300

SAIC
Science Applications International Corporation

SECURITY CLASSIFICATION OF THIS PAGE (When Data Entered)

REPORT DOCUMENTATION PAGE

READ INSTRUCTIONS BEFORE COMPLETING FORM

1. REPORT NUMBER: SAIC-85/1683	2. GOVT ACCESSION NO.: AD-A155559
3. RECIPIENT'S CATALOG NUMBER:	
4. TITLE (and Subtitle): Final Report on Contract N00014-83-C-0303	5. TYPE OF REPORT & PERIOD COVERED: Final Report 12/13/82 - 2/10/85
	6. PERFORMING ORG. REPORT NUMBER: SAIC-85/1683
7. AUTHOR(s): C.W. Spofford	8. CONTRACT OR GRANT NUMBER(s): N00014-83-C-0303
9. PERFORMING ORGANIZATION NAME AND ADDRESS: Science Applications International Corp. 1710 Goodridge Drive, P.O. Box 1303 McLean, VA 22102	10. PROGRAM ELEMENT, PROJECT, TASK AREA & WORK UNIT NUMBERS: Tasks 1, 2, 3 and 4
11. CONTROLLING OFFICE NAME AND ADDRESS: Naval Ocean Research and Development Activity NSTL Station, MS 39529	12. REPORT DATE: April 1985
	13. NUMBER OF PAGES:
14. MONITORING AGENCY NAME & ADDRESS(if different from Controlling Office): Office of Naval Research Dept. of the Navy 800 N. Quincy Street Arlington, VA 22217	15. SECURITY CLASS. (of this report):
	15a. DECLASSIFICATION/DOWNGRADING SCHEDULE:

16. DISTRIBUTION STATEMENT (of this Report)

Unlimited

17. DISTRIBUTION STATEMENT (of the abstract entered in Block 20, if different from Report)

18. SUPPLEMENTARY NOTES

19. KEY WORDS (Continue on reverse side if necessary and identify by block number)

Ocean acoustics, propagation, scattering theory, seafloor geology

20. ABSTRACT (Continue on reverse side if necessary and identify by block number)

This report summarizes work performed by SAIC under the Bottom Interaction Program on contract to NORDA. Tasks on this contract focused on understanding the coherence losses incurred by bottom-retained signals due to three mechanisms: sub-bottom roughness, random inhomogeneities in the sediment column, and partial reflections from near-surface layering in the sediment. Work in the

DD FORM 1 JAN 73 1473 EDITION OF 1 NOV 65 IS OBSOLETE

S/N 0102-LF-014-6601

TABLE OF CONTENTS

CONTRACT SUMMARY

This report summarizes work performed by SAIC on Contract N00014-83-C-0303 for the Bottom Interaction Program managed by NORDA. Four tasks were addressed in the course of this work:

Task 1 - Support the Bottom Interaction Program - Thin Sediment

Principal Investigator - C.W. Spofford

Task 2 - Analyze and Interpret Bearing Stake Coherence Data

Principal Investigators - L.B. Dozier
J.S. Hanna

Task 3 - Support the Bottom Interaction Program - Thin Layers

Principal Investigator - R.R. Greene

Task 4 - Investigate Spatial Coherence in Shallow Water

Principal Investigator - L.B. Dozier

Work on each of these tasks is summarized in the following sections. Separate SAIC reports have been generated to document the results of Tasks 2, 3, and 4. Work on Task 1 is on-going and has been continued in FY85 under a new contract. Two references generated under this effort are included here since they have to date received less distribution.

Task 1 - Support the Bottom Interaction Program - Thin Sediment

Summary

The objective of this task was to attempt to reconcile several different aspects of the problem of bottom interaction in the vast, thin-sediment regions of the Northeastern Pacific abyssal hills. Data from these areas suggested anomalous behavior of bottom-interacting signals in two ways:

1. Loss versus grazing angle at the acoustic basement - approximately 6 dB independent of grazing angle and frequency (from 50 to 1500 Hz); and

2. Very large time spreading of the signal - again largely independent of grazing angle and frequency.

In earlier work for the Bottom Interaction Program SAIC had developed a composite-roughness scattering theory which takes as input the bottom roughness spectrum and computes the fraction of energy scattered into specular and non-specular directions as a result of that roughness. In this task the first step was to obtain data on the basement roughness and see whether the observed roughness when used in this state-of-the-art scattering theory could account for the large observed time spreads. It was also hoped that an understanding of this scattering phenomenon might elucidate the peculiar total loss characteristics.

The work on this task has produced the following:

1. A paper summarizing the status of the bottom-loss and coherence problem with emphasis on the thin sediment behavior: "Status of the Bottom Loss Problem Relative to Bottom Bounce Coherence" by C.W. Spofford, published in the Precedings of the NAVSEA Stochastic Modeling Workshop, NAVSEA, C.W. Spofford and J.M. Haynes, eds., September 1983.

2. A paper on the statistics of basement roughness based on our analysis of Deep Tow data provided by Fred Spiess of Scripps: "Measurements of Basement Roughness and Sediment Thickness Statistics in Pacific Abyssal Hills," C.W. Spofford, E.S. Holmes and F.N. Spiess, submitted to Journal of Geophysical Research (1985).

Copies of these papers are attached for reference. The results presented in the second paper represent a fundamental extension of the data on bottom (or sub-bottom) roughness. In summary, the acoustical basement in this area northeast of Hawaii is composed of a rough chert layer lying approximately 40 m below the water-sediment interface. Our spectral estimates from Deep Tow blended in very smoothly with longer-wavelength estimates of bottom roughness reported by Bell. The spectral slope, however, steepened considerably (from $k^{-2.5}$ to $k^{-3.5}$ or more) in the two decades in wavelength that our new results spanned. Any attempts to extrapolate Bell's data beyond its limits would have been in significant error.

In the second part of this effort, this spectrum and the observed slope distributions were used in the composite-roughness and specular-scatter models, respectively, developed by SAIC to predict corresponding time spreads. Using the measured basement roughness, neither the low-frequency diffractive scattering model, nor the high-frequency optical scatterer model were able to yield time spreads as large as those observed. In fact no reasonable estimates for roughness which might be even plausible given the roughness data were able to produce long enough time spreads.

Work on this problem is continuing on a follow-on BIP contract on two fronts:

1. Horizontal and vertical array angle, frequency and time spread data from this area are being analyzed to better quantify the nature of the scatter both to support system performance estimates, and to provide insight into the effective scattering kernel of this bottom.

2. The acoustical properties of the chert, both its roughness scales (perhaps not measurable from Deep Tow) and its impedance characteristics are being investigated. Certainly over some of the area of interest chert is the effective basement.

In other parts, basalt is nearer the surface, however some DSDP data suggest that there may be chert very near this basalt. This may be a clue as to why scattering in the Pacific abyssal hills is so much stronger than in the Mid-Atlantic Ridge areas as reported by Ellinthorpe.

Task 2 - Analyze and Interpret Bearing Stake Coherence Data

A report entitled "Bearing Stake Coherence Analysis" (SAIC-85/1031) dated February 1985 was delivered under this task. The summary and conclusions from this report are as follows.

We compared results of a mode-based spatial coherence model with BEARING STAKE coherence measurements taken in a deep-water environment.

The model predicted excellent coherence in this situation; such excellent coherence is indeed seen in the best of the data. The apparently poor coherence in some of the data was evidently due to causes other than bottom interaction.

Task 3 - Support the Bottom Interaction Program - Thin Layers

A report entitled "A Random Layer Model for Reflection from Ocean Bottom Sediments" (SAIC-85/1036) dated February 1985 was delivered under this task. The conclusions from this report are as follows.

A procedure for estimating reflection losses from layered ocean bottom sediments, such as those observed in abyssal plains, was implemented. Limited experience with it indicates that it can reproduce observed reflection-loss levels using the geoacoustic properties and layering statistics of ocean bottom sediments. Furthermore, it reproduces the observed qualitative dependence of reflection loss on angle and frequency, including the negative frequency dependence.

Task 4 - Investigate Spatial Coherence in Shallow Water

A report entitled "Spatial Coherence in Shallow Water" (SAIC-85/1035) dated February 1985 was delivered under this task. The summary and conclusions from this report are as follows.

We compared model predictions of horizontal signal coherence loss due to bottom volume scattering with data from a shallow water experiment. Although we did not obtain quantitative agreement because of apparent rough-surface coherence loss included in the data, we were able to identify mode-stripping over the same-range intervals in both the model and the data. In addition, we developed a rule of thumb that, for this experiment at least, the optimal frequency for transmission was also relatively optimal for coherence.

REFERENCE A

STATUS OF THE BOTTOM-LOSS PROBLEM RELATIVE TO BOTTOM-BOUNCE COHERENCE

from

Proceedings of NAVSEA Stochastic Modeling Workshop, NAVSEA (1983)

STATUS OF THE BOTTOM LOSS PROBLEM RELATIVE TO BOTTOM-BOUNCE COHERENCE

C. W. Spofford
Science Applications, Inc.
1710 Goodridge Drive
P.O. Box 1303
McLean, Virginia 22102
(703) 821-4422

ABSTRACT

This paper attempts to summarize our current understanding of low-frequency bottom loss in order to set the stage for addressing the problems of bottom-bounce coherence. The bottom-loss problem in areas where sediments are thick seems to be well in hand. This understanding is demonstrated through comparisons of measured loss with simulated loss using a relatively simple geo-acoustic model. In thin sediment areas the loss is modelable, but with somewhat lower accuracy because large-angle scattering is so dominant. The data collected in these areas suggest three basic coherence problems:

1. Effects associated with fine, near-surface layering in the sediments,

2. Coherence losses due to random inhomogeneities in the sediment volume itself, and

3. Large-angle scattering and associated coherence problems when the sound interacts with the rough, hard basement in thin-sediment areas.

Work being performed at SAI in all three areas is summarized. (A subsequent paper by Dozier in these proceedings discusses the second problem in more detail.)

TABLE OF CONTENTS

Section 1
INTRODUCTION AND BACKGROUND

Before attempting to address the problem of bottom-bounce coherence, it is essential to have a clear picture for the dominant paths and loss mechanisms associated with bottom-interacting signals. Substantial progress has been made in this area under the auspices of the NAVELEX Bottom Interaction Program administered by NORDA. In fact, the understanding of loss mechanisms has reached the point that an Advanced Development, global, geo-acoustic bottom-loss model (BLUG) is being developed by SAI to support routine Fleet predictions. This paper attempts to summarize our current understanding of the bottom-loss problem and suggests certain priorities for bottom-bounce coherence.

The bottom-loss problem has been historically divided into analysis of phenomena where the sediments tend to be thick (greater than ~300 meters) or thin (loss than ~100 meters). In these two categories bottom loss and coherence are expected to have substantially different characteristics. In intermediate-thickness areas a mix of characteristics is expected. Sections 2 and 3 describe loss in thick and thin sediments, respectively. Section 4 summarizes on-going work at SAI in modeling the coherence of these signals.

Acknowledgments

Preparation of this paper was supported by the Naval Sea Systems Command. The Bottom Loss Upgrade (BLUG) work was sponsored by the SEAS and TAEAS Programs, and the coherence work by the Bottom Interaction Program.

Section 2
BOTTOM LOSS IN THICK SEDIMENT AREAS

The development of a global geo-acoustic model has depended upon the successful interpretation of a vast body of bottom-loss measurements. Figures 1-4 illustrate four examples of bottom-loss data collected by NADC in areas of thick sediments. One-octave bands were used about the indicated center frequencies and enough data were collected th : the curves represent median values in 2° bins in grazing angle. These data are discussed in much more detail in Reference 1.

These data contain several consistent features and a few artifacts of the measurement geometry. Examples of artifacts are the negative losses at very low grazing angles (Figure 1), and much of the structure at low frequencies and low grazing angles (Figures 1, 2 and 3). A prominent feature in many of the data is the rapid increase in low-frequency loss around 30-40 degrees grazing. This feature is not an artifact, but a mani station of the fact that the intense, shallower angle paths are not reflecting from the water-sediment interface, but are, in fact, being returned by refraction at depth in the sediments. Figure 5 illustrates the ray geometry for this case. The reflected rays are indicated by dashed rays, and inside the caustic range, R_c, only reflected rays are present. This leads to the second prominent feature of the data: the relatively angle- and frequency-independent character of the losses for angles greater than 30-40 degrees. There is observed some non-trivial frequency dependence (discussed in more detail in

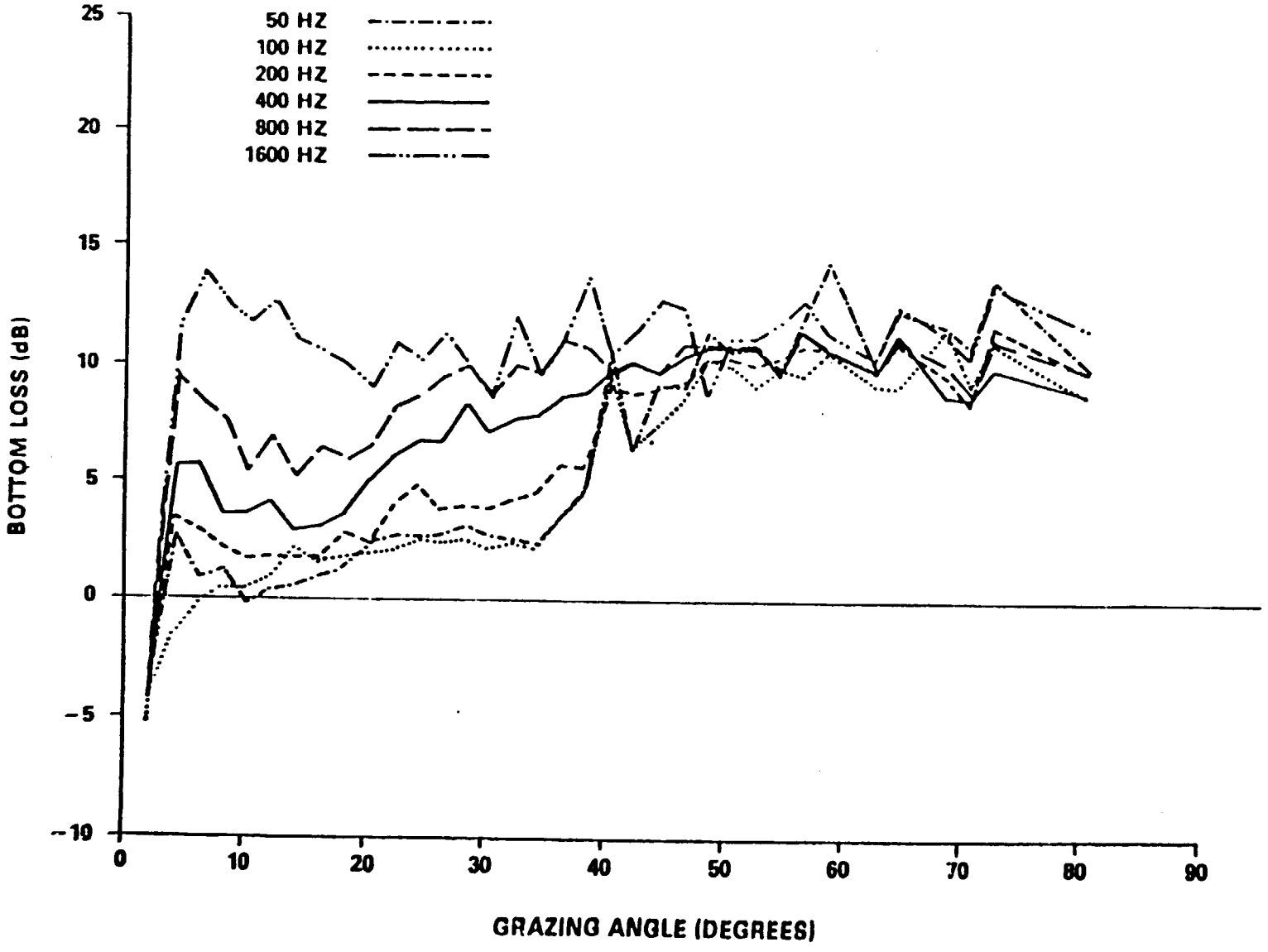

Figure 1. Bottom loss versus grazing angle measured in six one-octave bands at indicated center frequencies: zero high-angle frequency dependence.

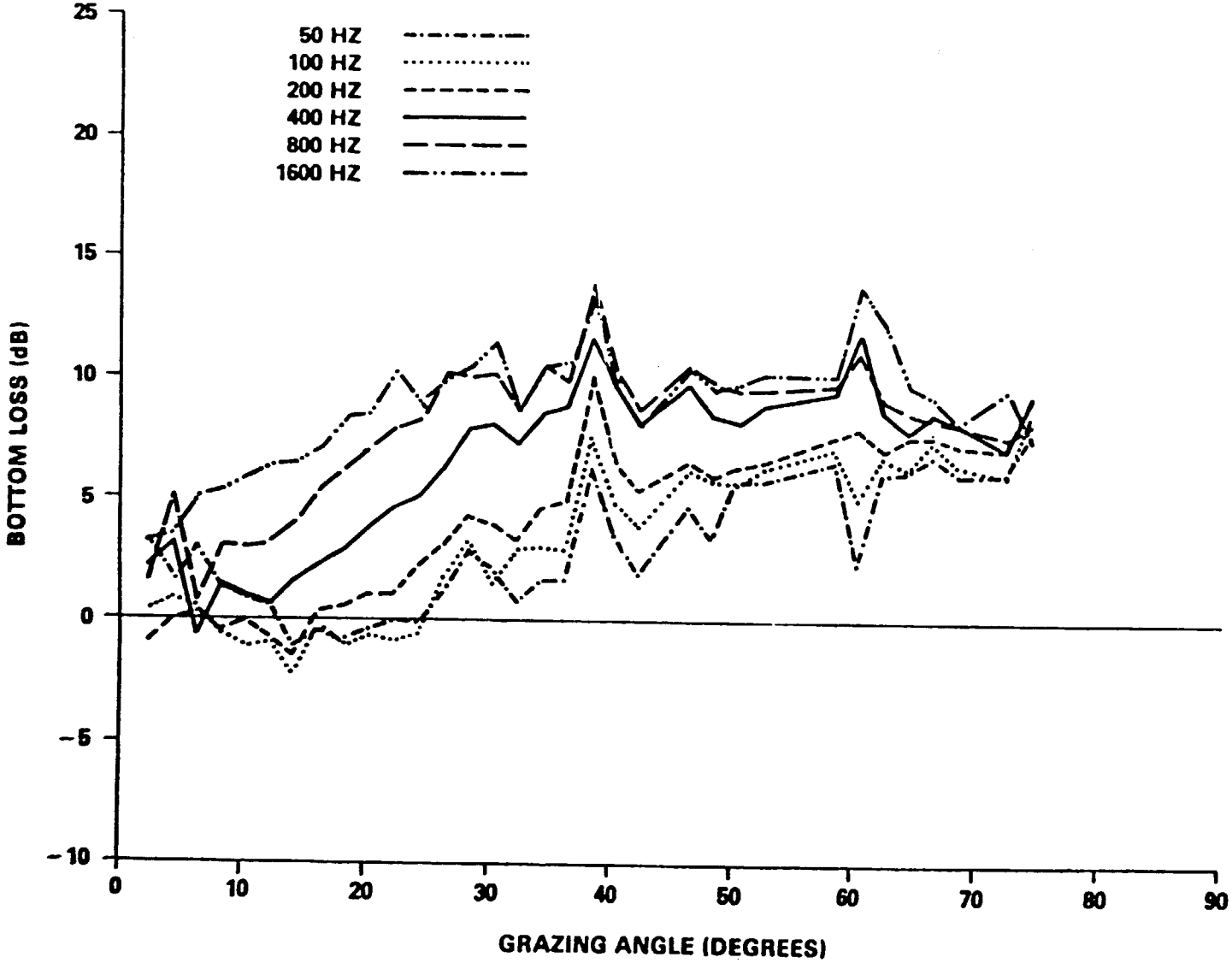

Figure 2. Bottom loss versus grazing angle measured in six one-octave bands at indicated center frequencies: positive high-angle frequency dependence.

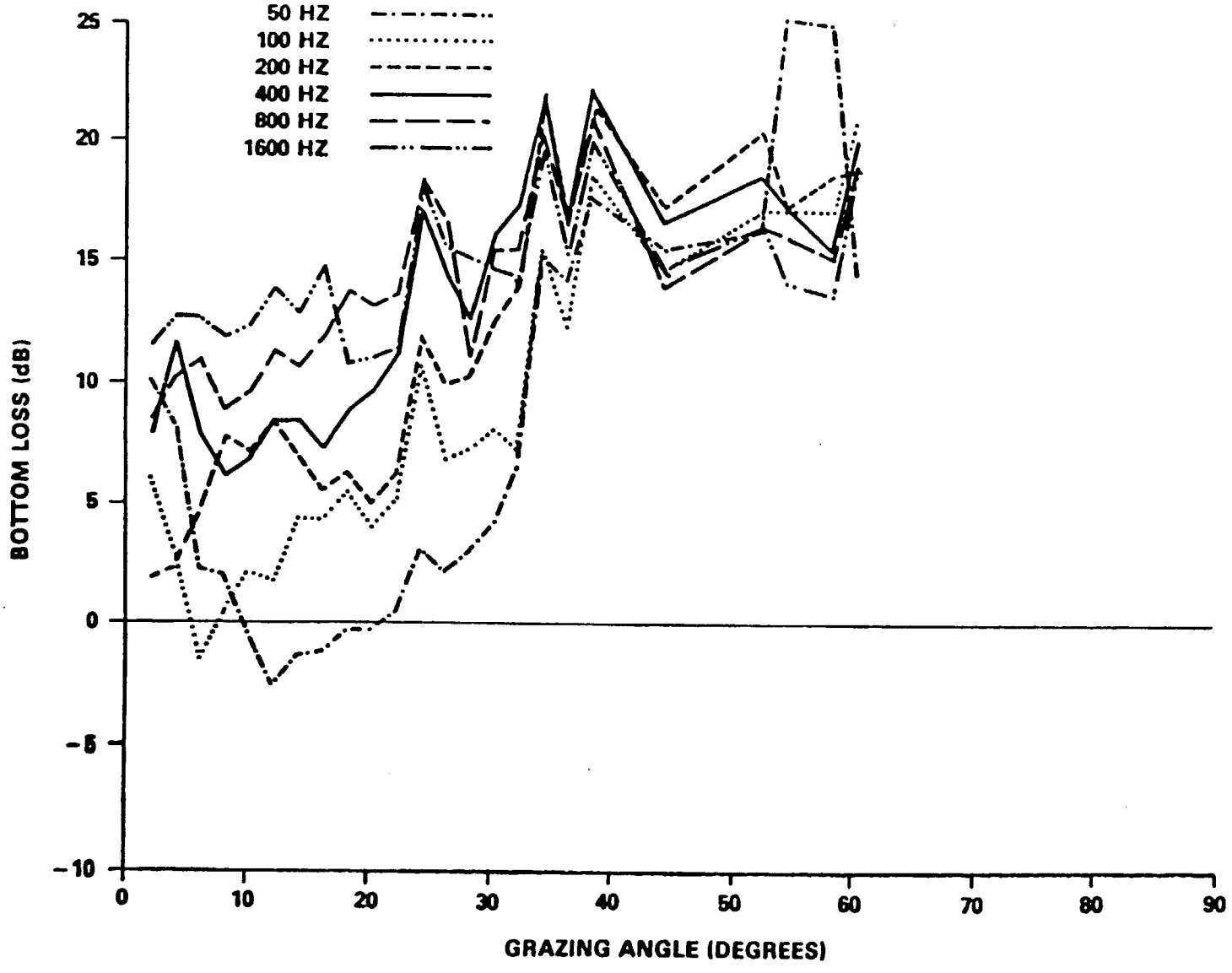

Figure 3. Bottom loss versus grazing angle measured in six one-octave bands at indicated center frequencies: negative high-angle frequency dependence.

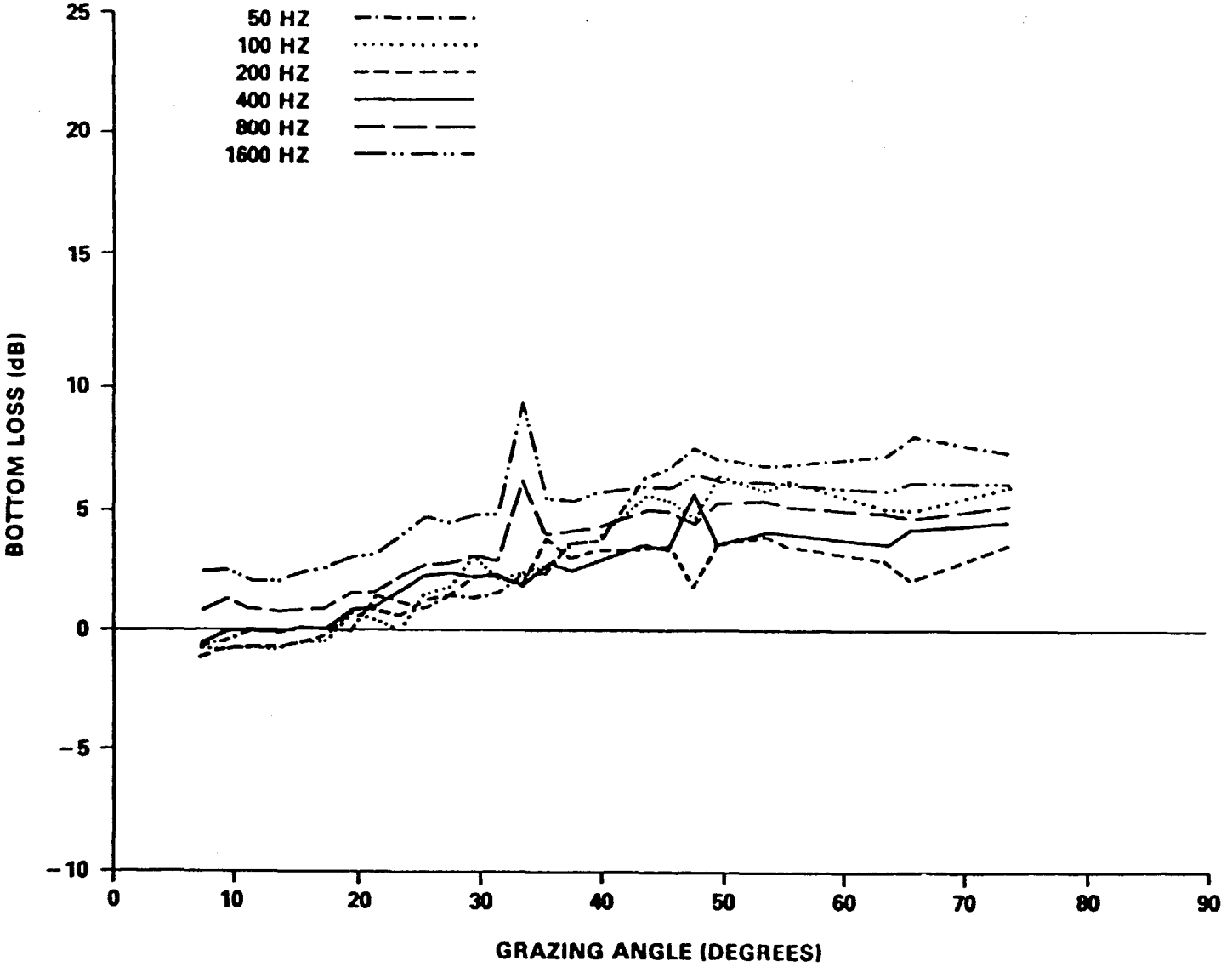

Figure 4. Bottom loss versus grazing angle measured in six one-octave bands at indicated center frequencies: reversing high-angle frequency dependence.

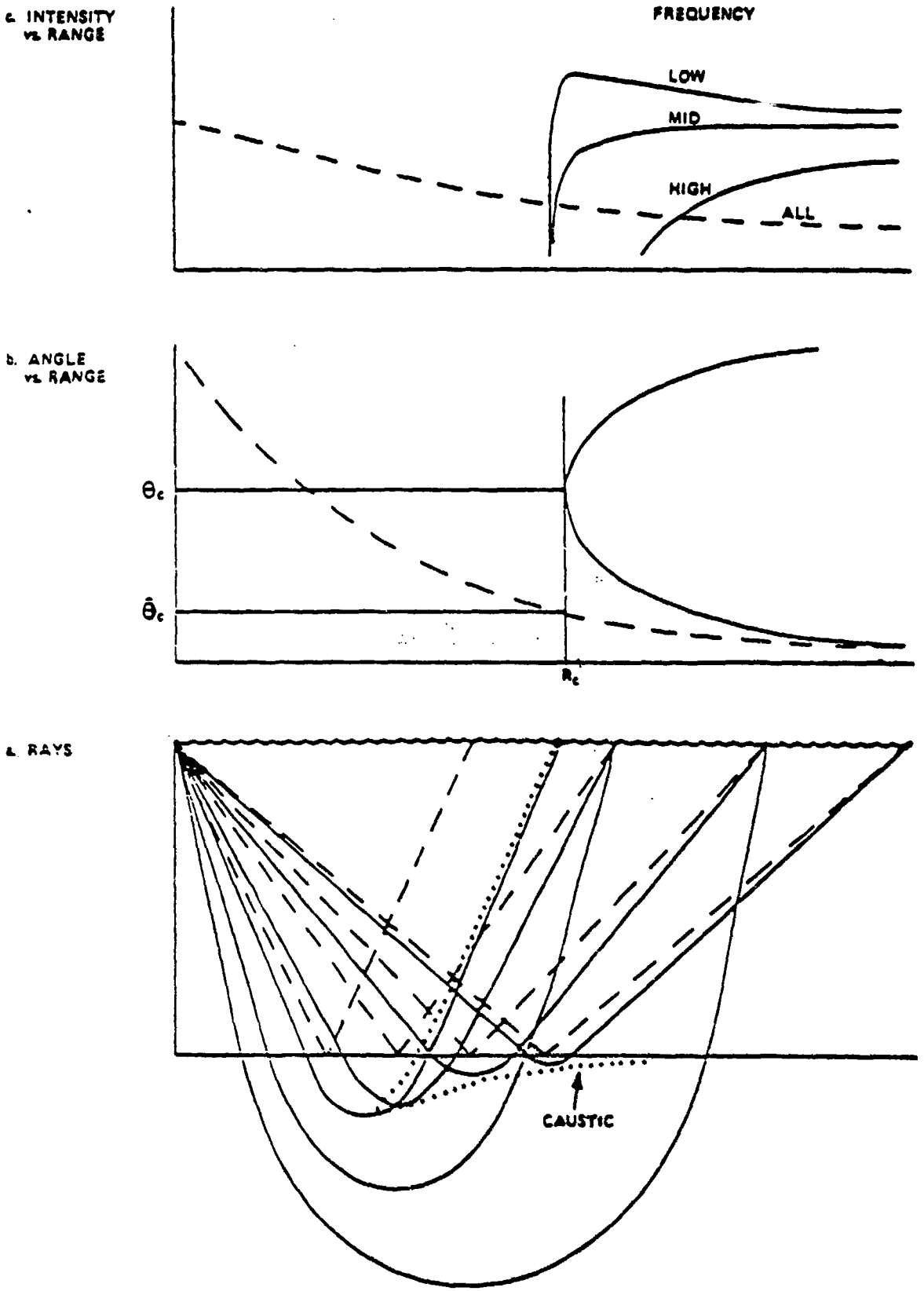

Figure 5. Ray geometry (a), angle (b) and intensity (c) versus range for reflected (---) and refracted (——) paths where the refracted paths form a caustic (···) in the sediment.

Reference 1) reflecting either the presence of basement, and/or the effects of near-surface layering in the sediments.

When one examines time series of the shots used to collect these data, this interpretation is reinforced. Figure 6 illustrates the low pass (<2 kHz) impulse response of the returned wave, aligned to the first return and plotted versus grazing angle.[2] The refracted arrival seems weak compared to the initial, reflected arrival, however when this time series is low-pass (40-90 Hz) filtered (Figure 7), the refracted arrival is seen to dominate.[2] The presence of near surface fine-layering is seen in the early structure in Figure 6. The constant spacing in time between these micro-arrivals suggests spatially homogeneous layers. In these data the corresponding bottom-loss measurements actually show somewhat less high-angle loss at high frequencies than at the lower frequencies which essentially don't "see" this layering (Figure 7).

The NADC data set of several hundred bottom loss measurements were successfully interpreted this way in the context of a simplifed geo-acoustic model for the sediments (Figure 8). By examining various parts of the bottom-loss versus grazing-angle curves, estimates were made of the sound-speed and attenuation profiles, plus apparent surface impedances and some aspects of the near-surface layering. Figures 9-12 illustrate the comparisons of data (x) with simulated bottom loss (including estimated measurement artifacts) for four data sets.[1] These curves progress through higher and higher apparent surface impedances (much higher than the actual sound-speed/density contrast at the water-sediment interface would suggest), indicating that even at

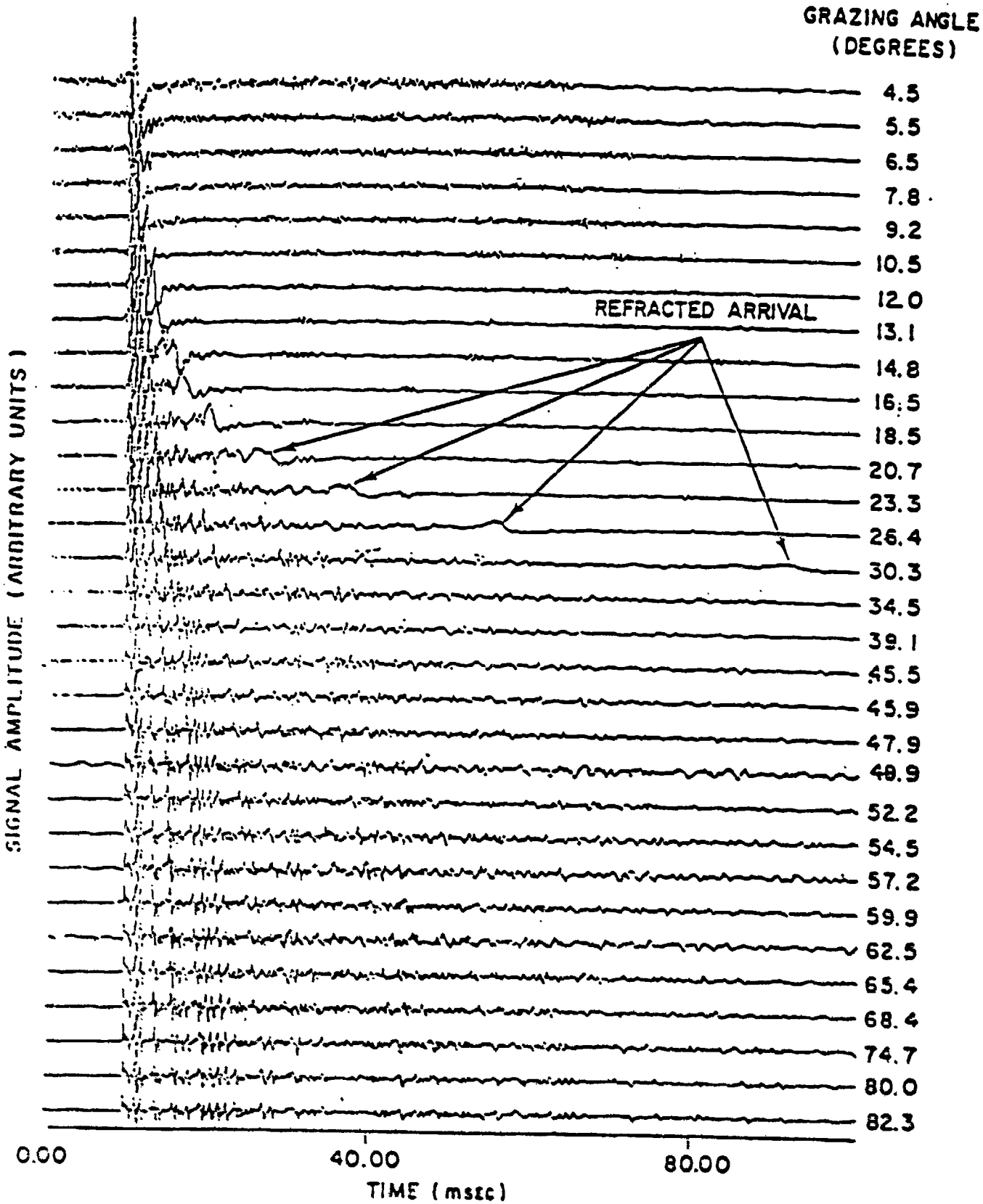

Figure 6. Impulse response Gaussian low-pass (2 kHz) filtered signal structure obtained by deconvolution, thick sediments.[2]

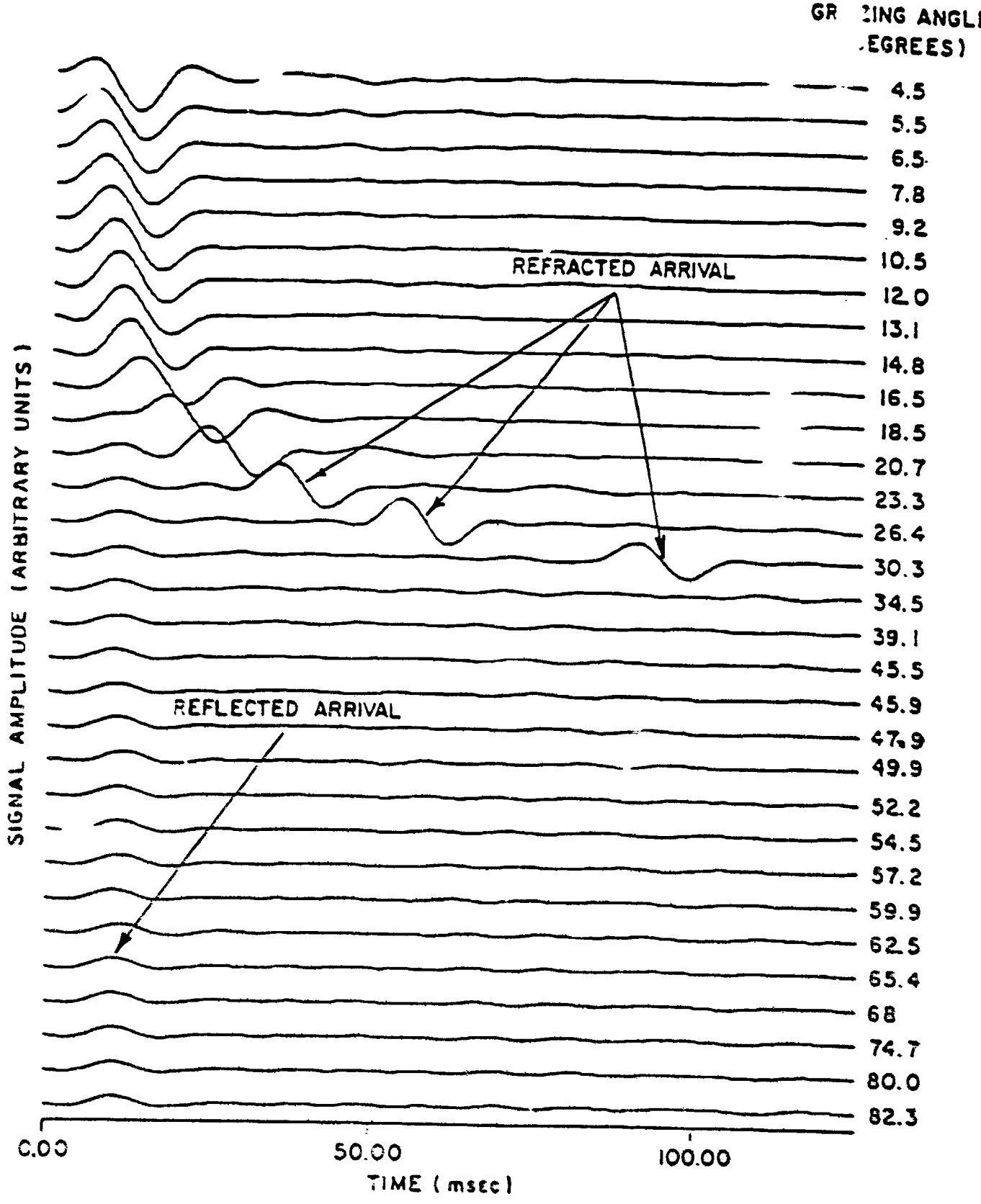

Figure 7. Low-pass (40-90 Hz) filtered impulse responses corresponding to Figure 6 illustrating reflected and refracted arrivals.[2]

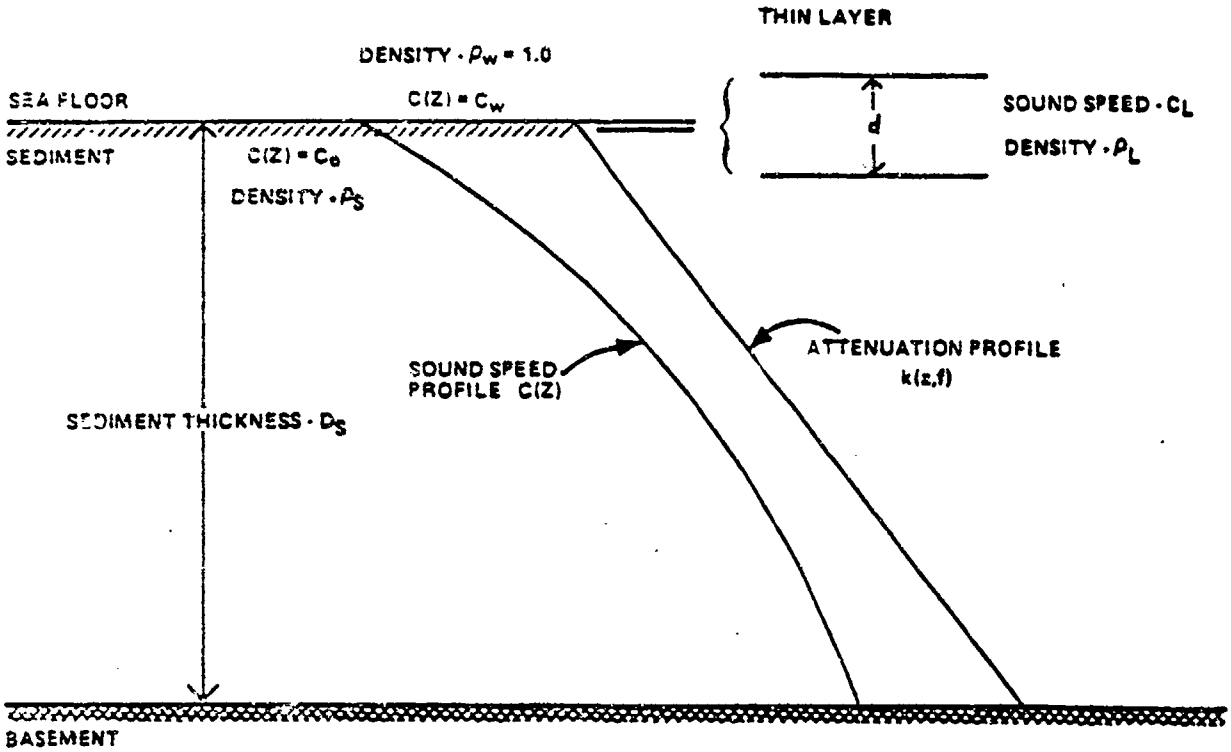

Figure 8. Simplified geo-acoustic model used in BLUG.

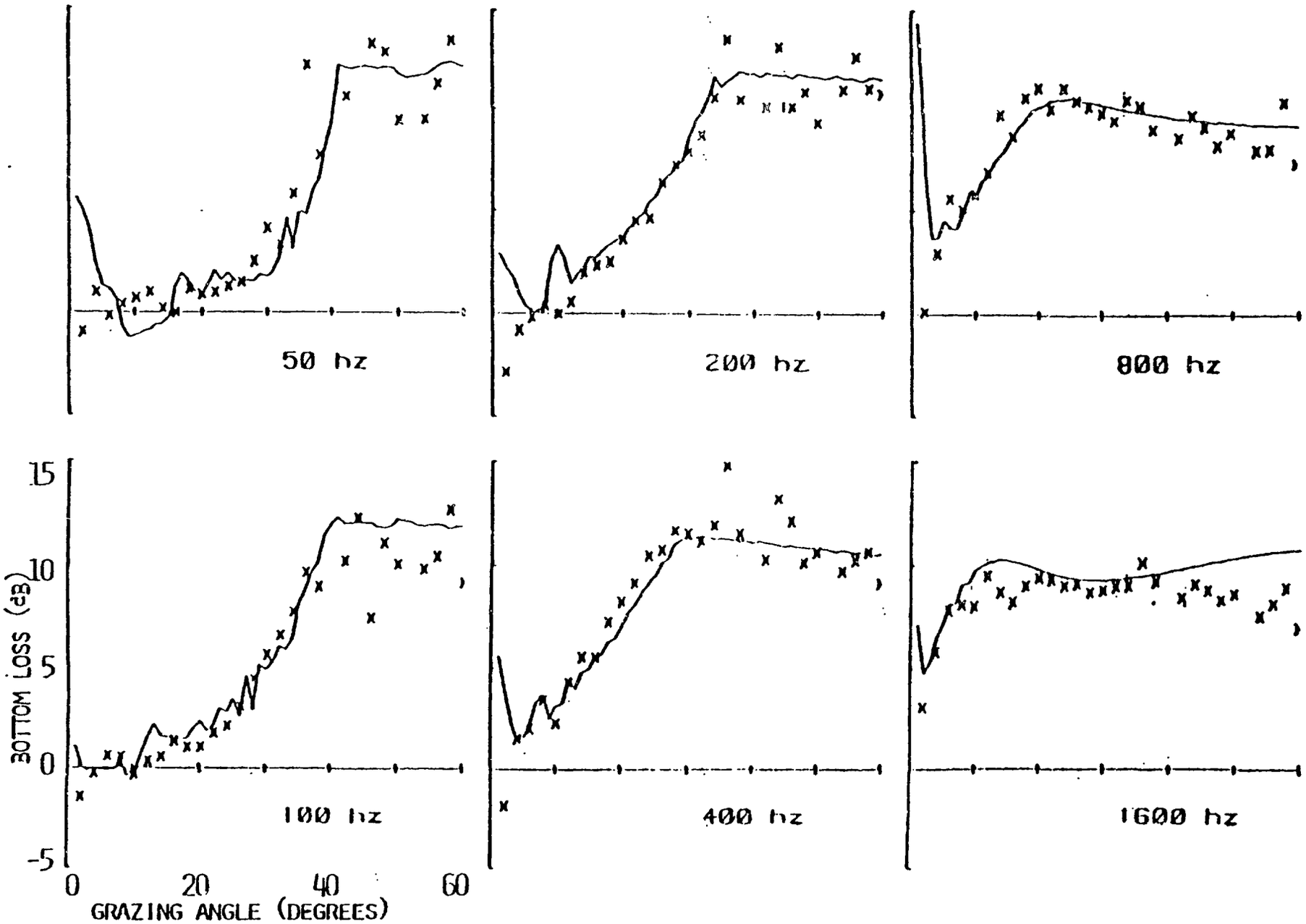

Figure 9. Comparison of simulated (——) and measured (X) bottom-loss for one-octave bands at six center frequencies: calcareous sediments, typical negative frequency dependence.

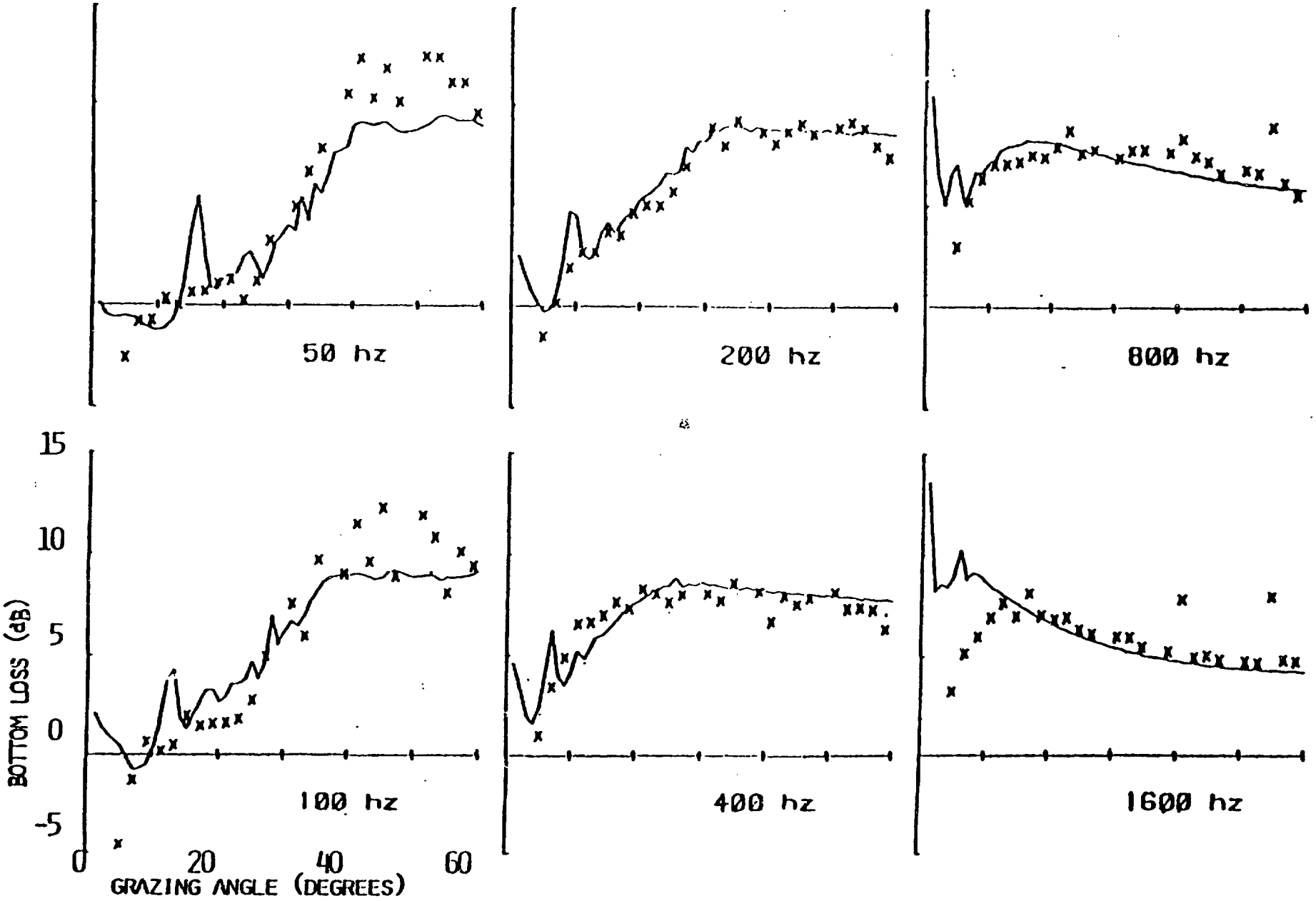

Figure 10. Comparison of simulated (——) and measured (X) bottom-loss for one-octave bands at six center frequencies: calcareous sediments, strong negative frequency dependence.

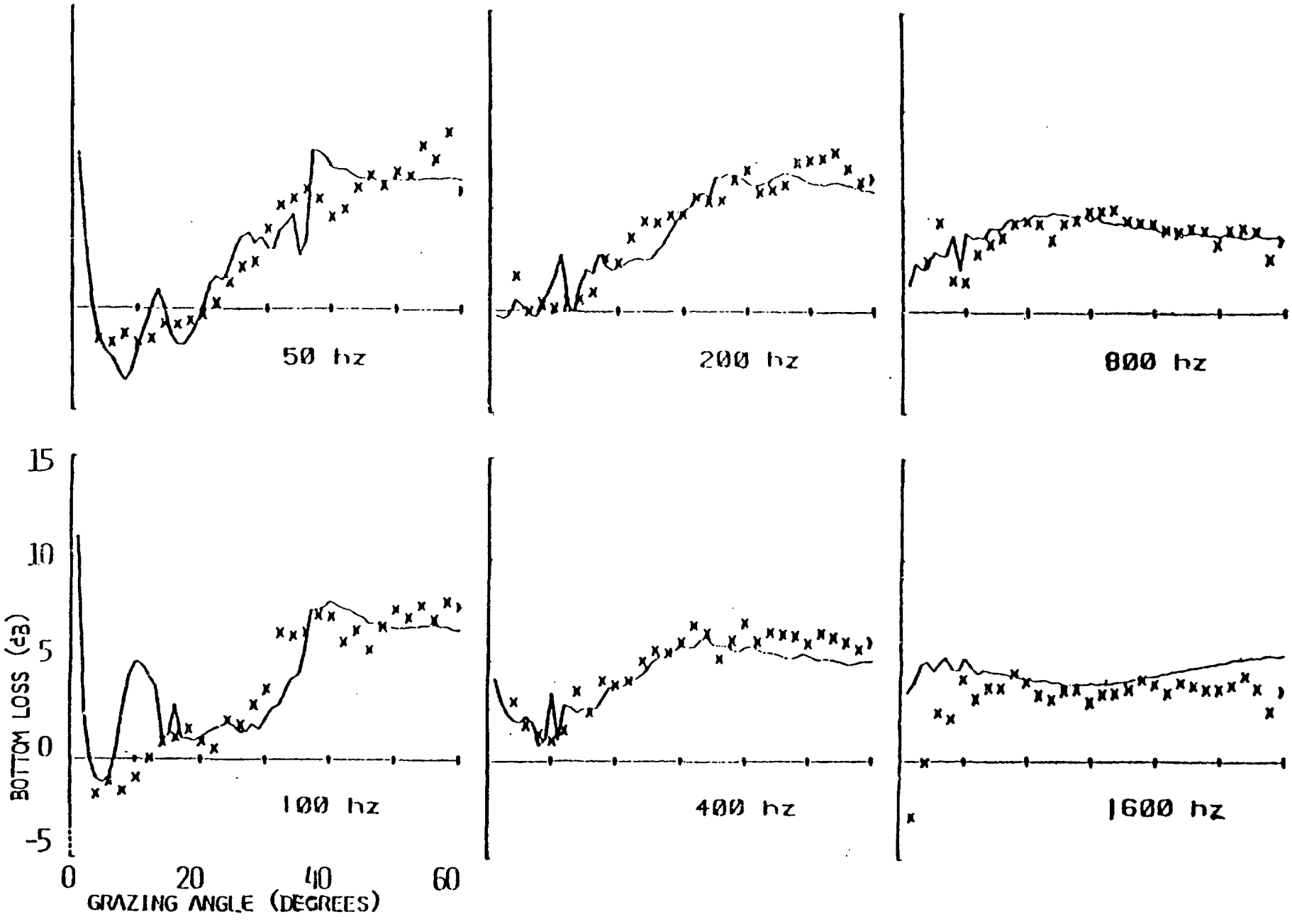

Figure 11. Comparison of simulated (——) and measured (X) bottom-loss for one-octave bands at six center frequencies: terrigeneous sediments, low-speed bottom, severe negative frequency dependence.

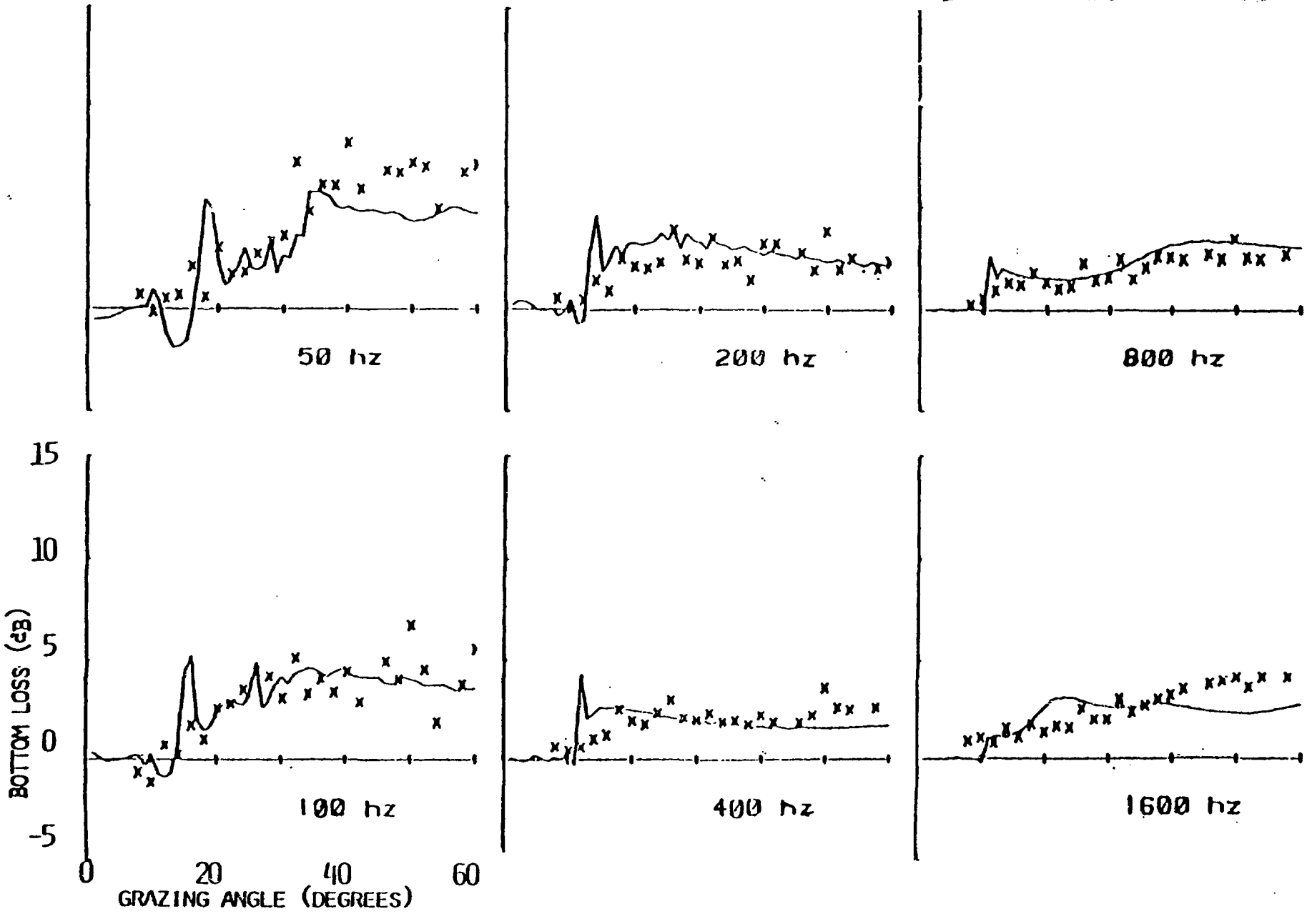

Figure 12. Comparison of simulated (——) and measured (X) bottom-loss for one-octave bands at six center frequencies: terrigenous sediments, high-speed bottom, severe frequency reversal.

low frequencies, near-surface layering may be quite important.

In summary, the behavior of loss in thick-sediment areas is dominated by the following features:

1. For low frequencies and angles shallower than the apparent angle of the caustic emerging from the bottom (30-40 degrees), the field is controlled by the deep-refracting path.

2. At higher frequencies for the same angles, the more highly attenuated refracting path becomes dominated by the near-surface reflected path, at an angle which depends on the layering characteristics.

3. At higher grazing angles the field is controlled by the near-surface properties, including layering, and may exhibit a fairly complicated frequency dependence with only slight angle dependence.

4. As sediments get thinner (Figure 2) the basement reflected return may dominate the low-frequency high-angle loss. (For very thin sediments this return may dominate even up to 1 kHz as discussed in the following subsection.)

Section 3
BOTTOM-LOSS IN THIN-SEDIMENT AREAS

The same bottom-loss simulation model has been run against bottom-loss data collected in several areas of the Pacific where the sediments tend to be approximately 40 meters thick. Figures 13-15 illustrate some examples of these comparisons which tend to show less agreement for several reasons discussed below.[3] The data generally show less loss at lower frequencies and very little obvious angle dependence, except at very shallow grazing angles where the path can refract above the basement.

In these thin-sediment areas the basement is quite rough and large-angle scattering is expected. Figure 16 illustrates the aligned low-pass (<1 kHz) impulse response from such an area.[4] Note the time-axis scale change over Figures 6 and 7. The signal is reverberant from the bottom, lasting well over a second. At low frequencies (Figure 17) the signal lasts just as long with no dominant path.[4] The scattering must be quite diffuse, since the "specular" (first) return contains very little energy.

The fact that the time spreads at low and high frequencies are similar suggests that these returns cannot be coming from great depths in the basement itself (or no high-frequency returns would be seen). Hence the signal must be coming from the sediment/basement interface (energy analysis shows it cannot be a pure sediment-reflected return). When the observed time spread is translated into the corresponding area on the bottom from which the signal must be coming (Figure 18), the constant time-spread ellipses covering 1 to

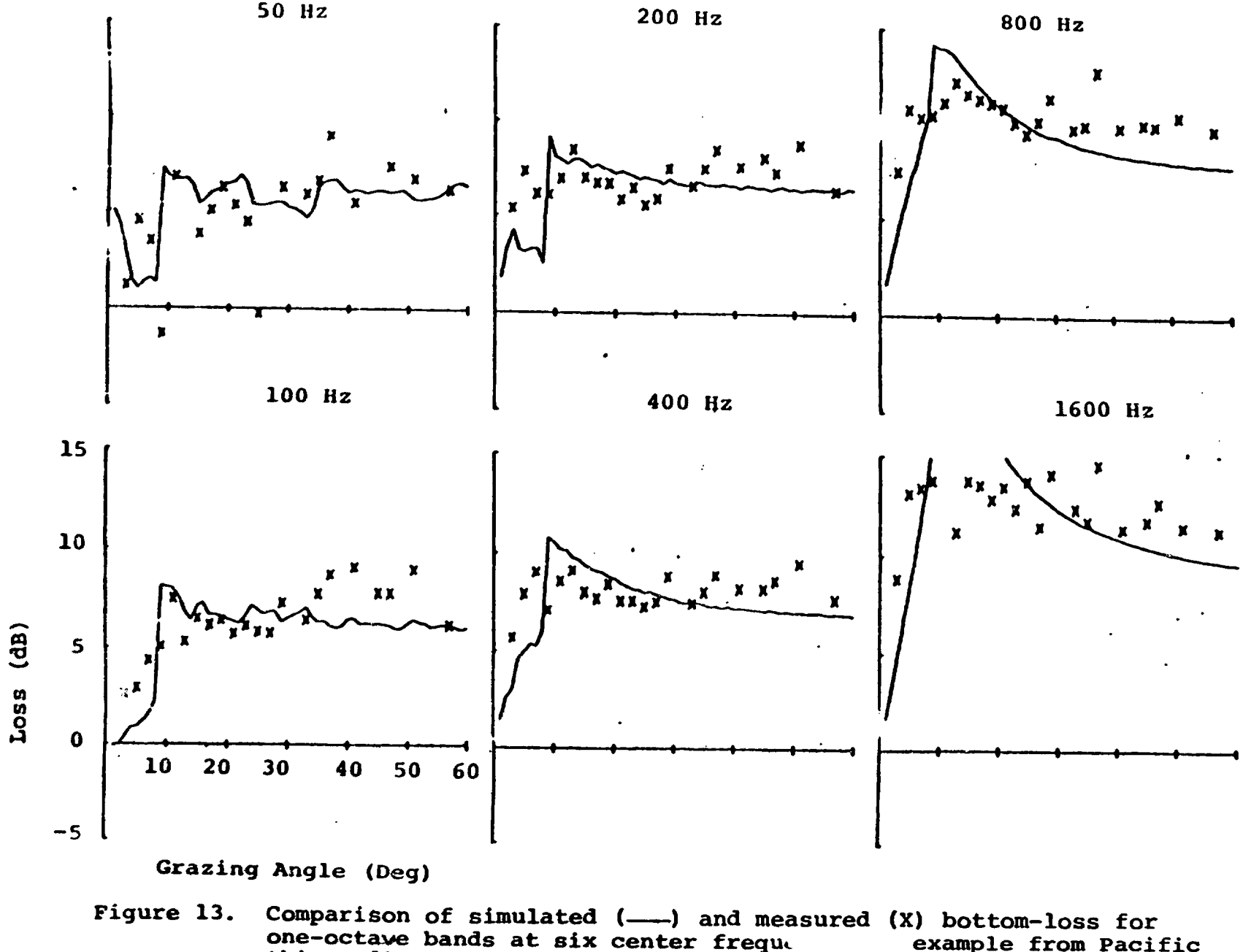

Figure 13. Comparison of simulated (——) and measured (X) bottom-loss for one-octave bands at six center frequ example from Pacific thin sediment area.

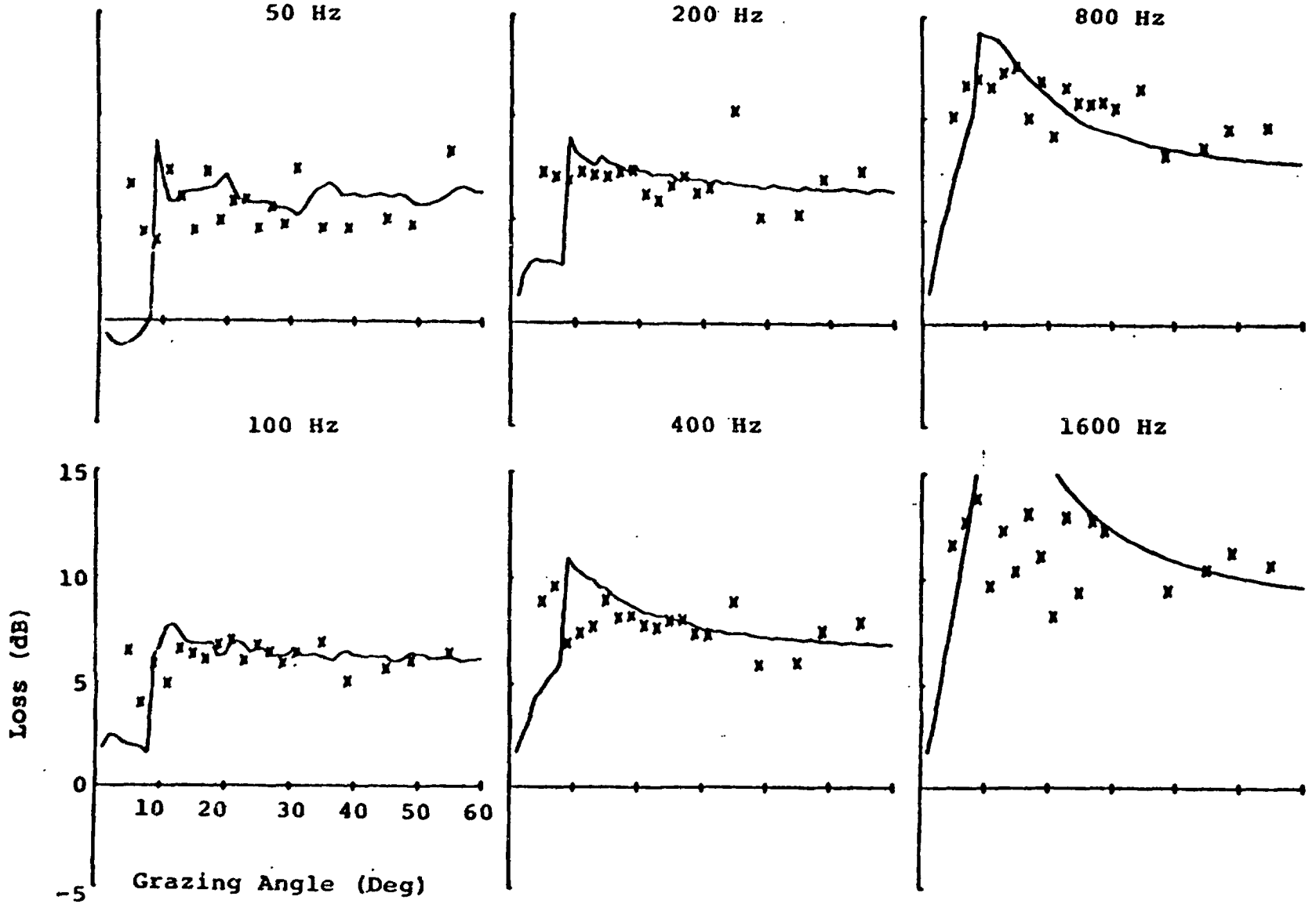

Figure 14. Comparison of simulated (——) and measured (X) bottom-loss for one-octave bands at six center frequencies: example from Pacific thin sediment area.

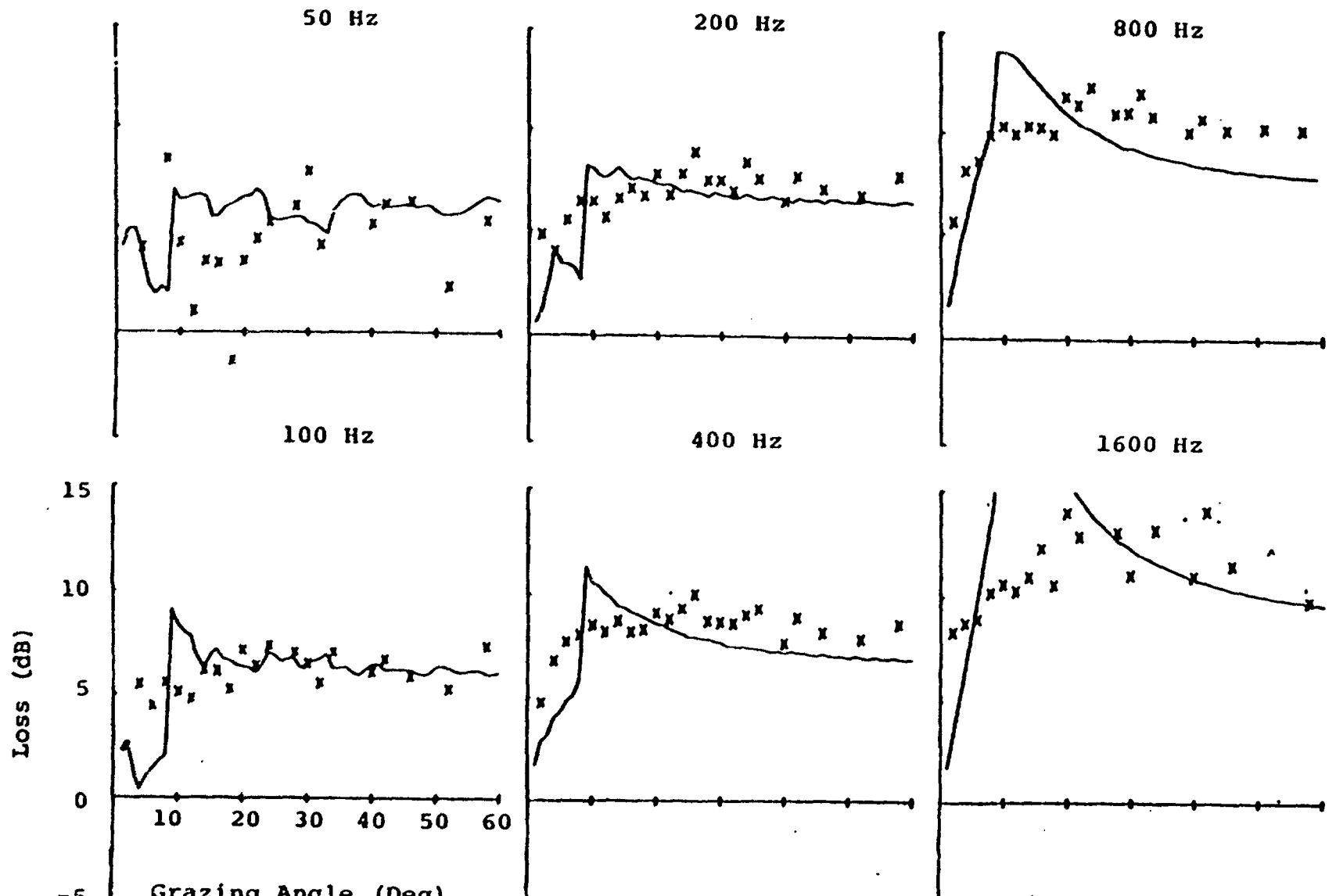

Figure 15. Comparison of simulated (——) and measured (X) bottom-loss for one-octave bands at six center frequencies: example from Pacific thin sediment area.

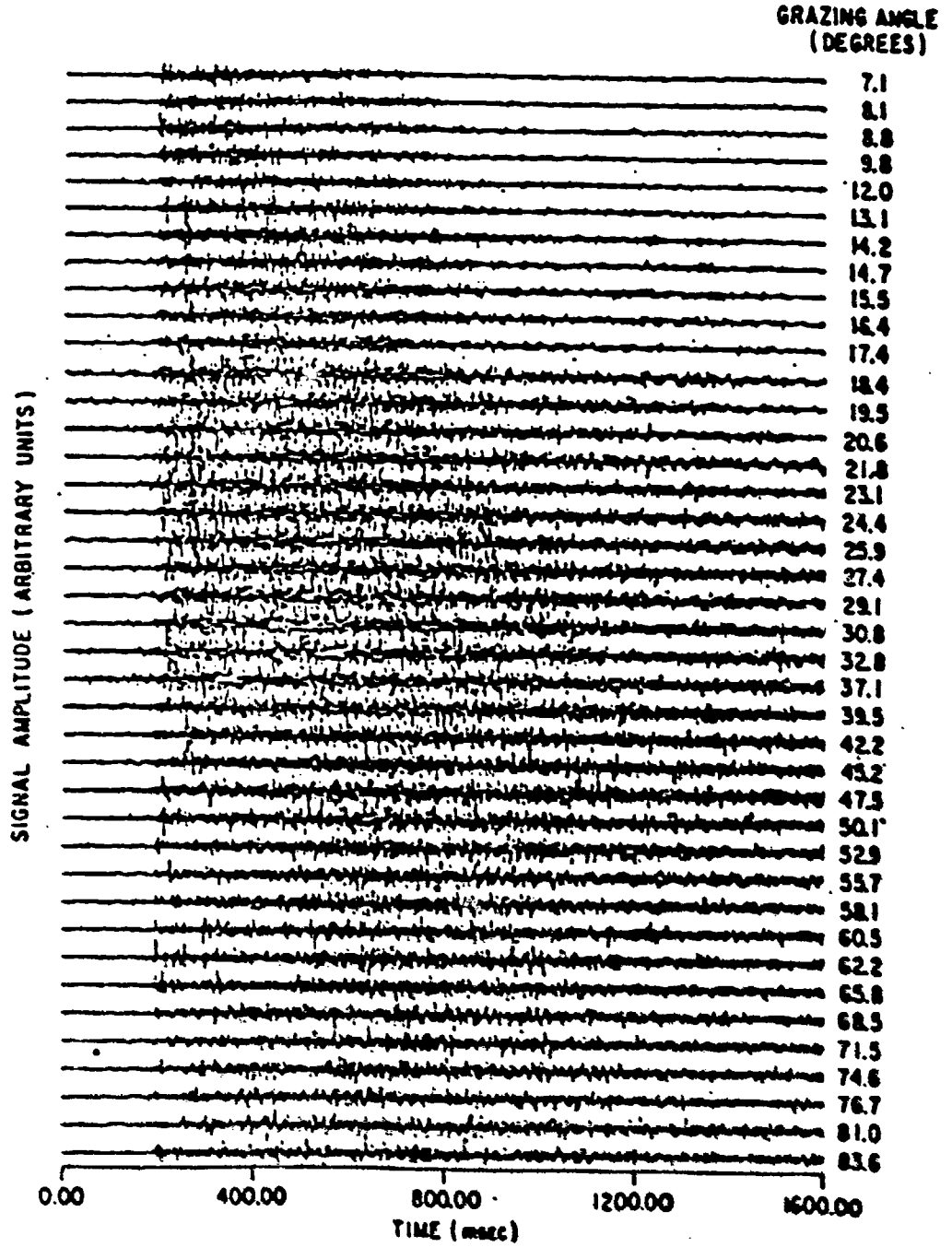

Figure 16. Bottom impulse response for a thin sediment location in the eastern Pacific, low-pass filtered at 1 kHz.

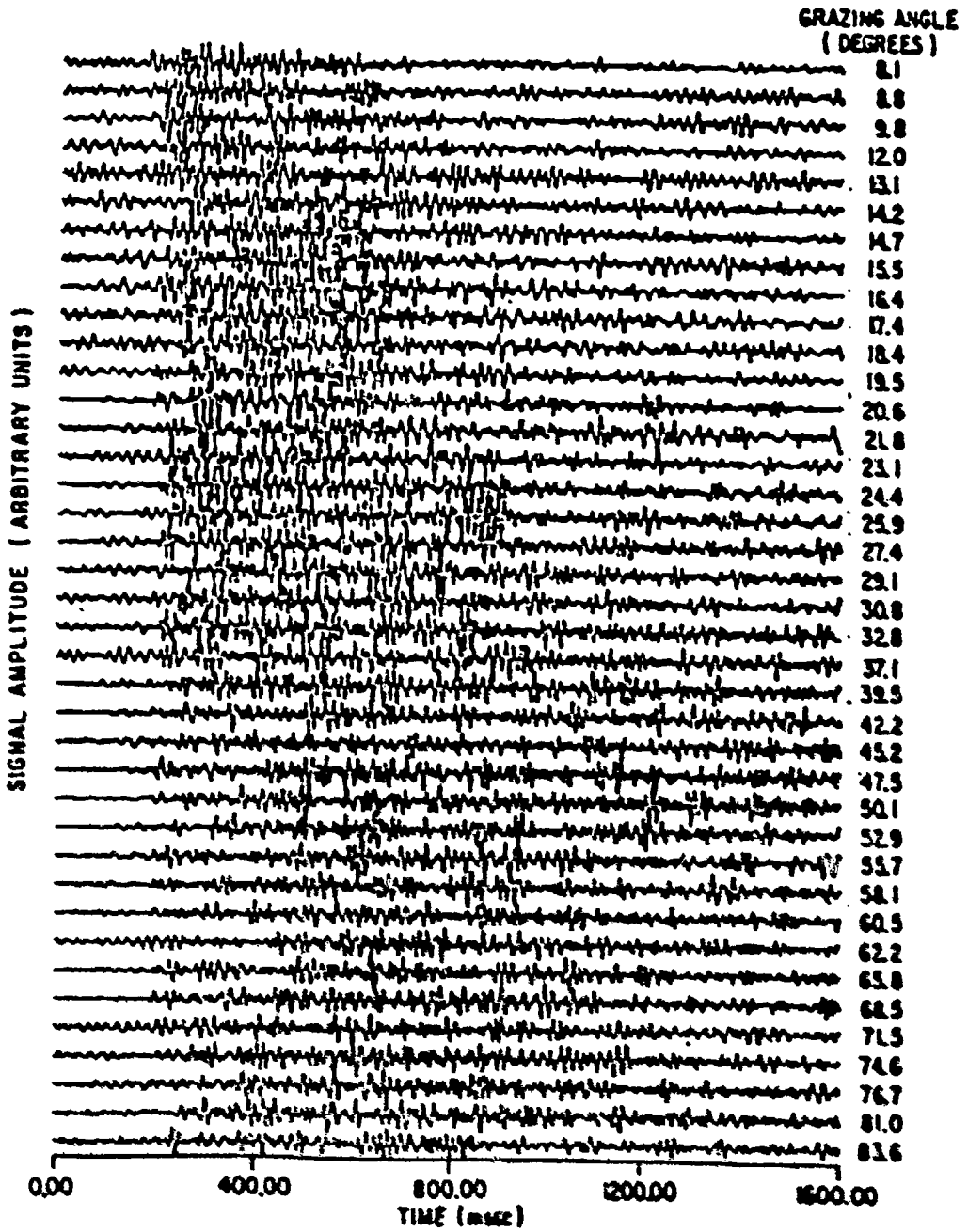

Figure 17. Bottom impulse response for a thin sediment location in the eastern Pacific, band-pass filtered from 40-90 Hz.[4]

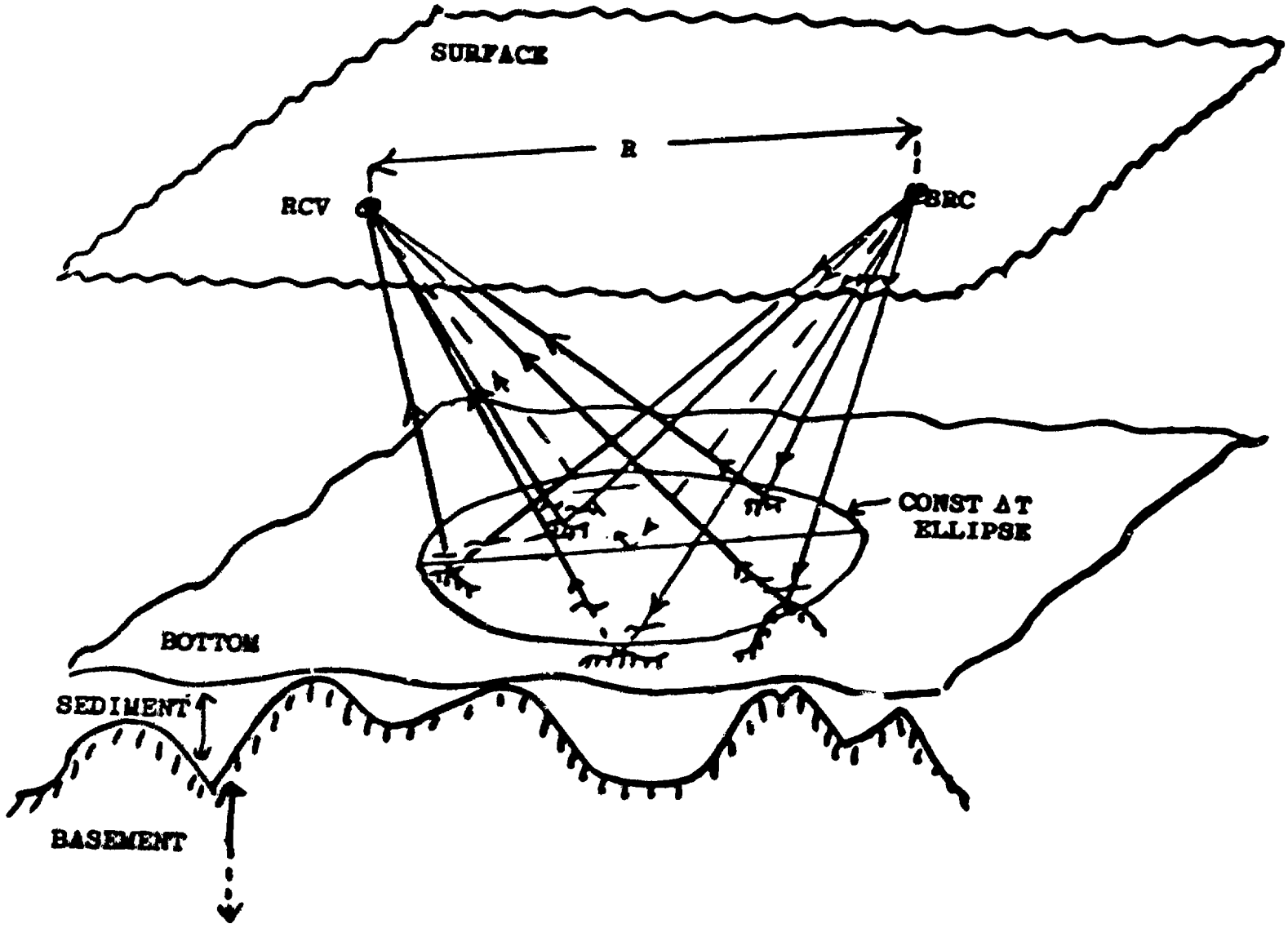

Figure 18. Reverberant bottom-bounce signal in a thin-sediment area.

1.5 seconds are quite large. Hence the bottom-reflected signal is spread in both azimuthal and depression angles as well as time. If the source and/or receiver of Figure 18 were moving, these angular spreads would result in a frequency spread for a cw signal due to differential Doppler on the angularly spread components. The following section discusses these coherence issues in more detail.

Section 4
COHERENCE MODELING

Figure 19 summarizes the three bottom-interaction coherence problems SAI is currently pursuing in the Bottom Interaction Program. In thick-sediment areas two issues are being addressed:

1. The loss and temporal spread of signals reflected by the near-surface layering. Greene has just begun work on this problem. In his model the layering is treated as a discrete, jump (Poisson) process with very large (effectively infinite) horizontal correlation lengths. Besieris and Kohler[5] are treating the same problem with continuous layering (which may be slightly less physical), but with a finite horizontal correlation length.

2. The spatial coherence (angular spreads) of the refracting path associated with random inhomogeneities in the bulk of the sediment. (Dozier discusses this problem in more detail in a subsequent paper.)

In thin-sediment areas the loss and coherence problems are not so easily separated. Our work in this area addresses all spreads as well as total loss. The approach uses a transport-equation model to construct the average intensity as a function of angles (θ,ϕ) and time (t) for a given range (R) and frequency (f):

THICK SEDIMENTS

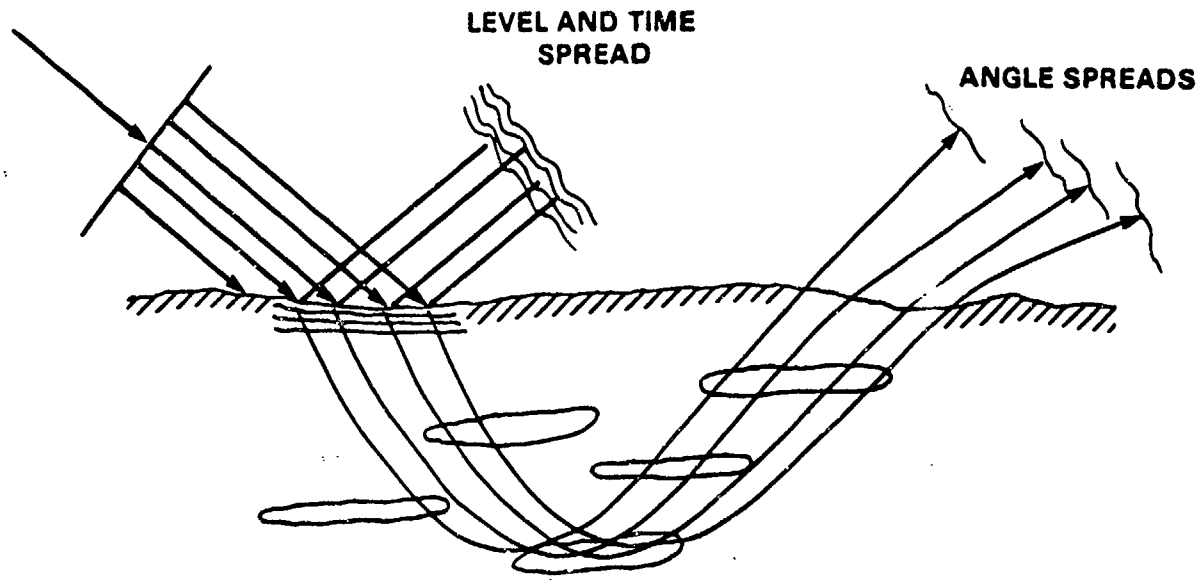

THIN SEDIMENTS — ROUGH BASEMENT

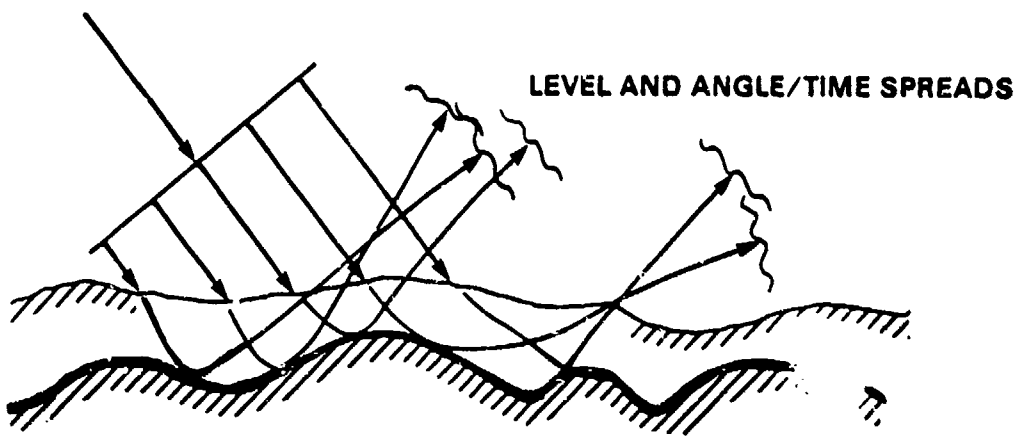

Figure 19. Three bottom interaction coherence problems.

$$I(\theta,\phi,t;R,f)$$

Transforms of this spread function yield the spatial and frequency mutual coherence functions.

In terms of observables and sonar equation parameters, for a cw signal (static source and receiver)

$$I_1(\theta,\phi) = \int_t I(\theta,\phi,t)\, dt$$

defines the angular spectrum of the signal and a corresponding beam output for steered direction θ_s,ϕ_s would be

$$I_B(\theta_s,\phi_s) = \int_\theta \int_\phi I_1(\theta,\phi)\, BP(\theta,\phi;\theta_s,\phi_s)\, d\theta d\phi$$

where BP is the beam pattern for the steered direction. (For a moving source/receiver the corresponding frequency spread would be given by the differential Doppler on these spread angles computed at both ends, if necessary.)

To compare with impulse response data similar to Figures 16 and 17 we integrate over angle

$$I_t(t;R,f) = \int_\theta \int_\phi I(\theta,\phi,t;R,f)\, d\theta d\phi$$

Because scattering is so dominant, any model for the total loss must be consistent with these observed spreads.

The computation of this basic intensity spread $(I(\theta,\phi,t))$ is being done by a brute-force approach in which the bottom is divided into small areas related to the source and receiver by two grazing angles (θ,θ') and a bistatic scattering angle $(\Delta\phi)$. (The bottom roughness spectrum is taken to be isotropic, hence only $\Delta\phi$ is important.) These paths are related through refraction in the sediment to the corresponding basement angles (θ_b,θ_b'), and appropriate (frequency-dependent) attenuation losses in the sediment are accumulated.

The power scattered from θ_b into θ_b'- $\Delta\phi$ is computed using a composite-surface scattering kernel developed by Brown (Figure 20).[6] The composite-surface theories recognize that the large-angle scattering from a surface is controlled by the portion of the surface spectrum where the acoustical (k_0) and surface wavenumbers are comparable (basically diffractive Bragg-like scatter). These "diffraction" gratings are essentially carried on the large (long-wavelength) surface which introduces tilts to the gratings and, at high-frequencies, can shadow parts of the surface. The analysis is done in terms of these two surfaces which are separated spectrally at k_*, which depends on k_0. The results are fairly insensitive to the precise value of k_*.

The corresponding scattering kernel then transitions smoothly between the physical optics (high-frequency) and diffractive (low-frequency) limits. We are in the process of applying this model to analyze several data sets both for loss and measured spreads.

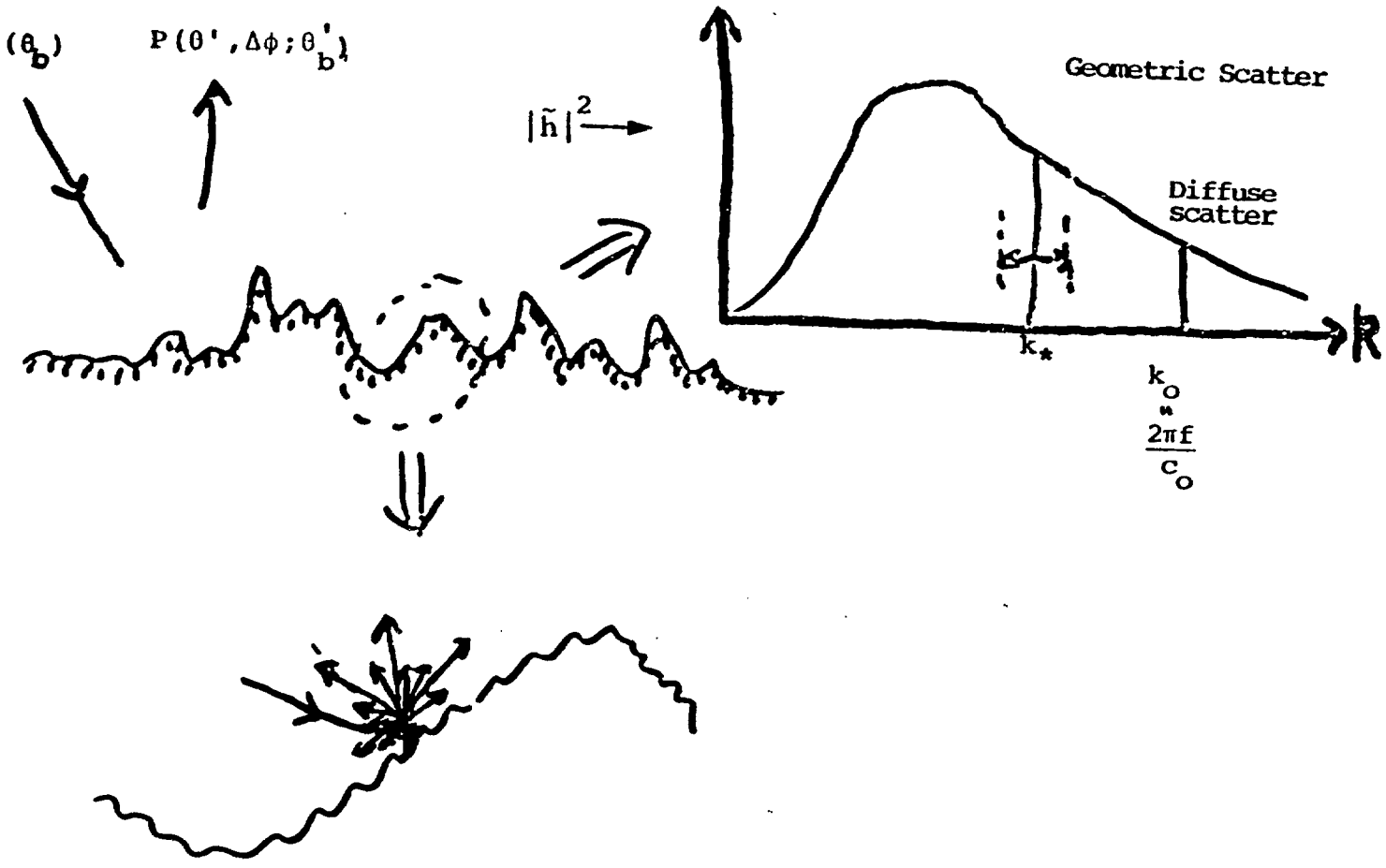

Figure 20. Composite-surface scattering from basement.

REFERENCES

1. C. W. Spofford, R. R. Greene, and J. B. Hersey, "The Estimation of Geo-Acoustic Ocean Sediment Parameters from Measured Bottom-Loss Data," SAI-83-879-WA (March 1983), submitted to JASA.

2. R. L. Dicus, "Preliminary Investigations of the Ocean Bottom Impulse Response at Low Frequencies," U.S. Naval Oceanographic Office, TN 6130-4-76 (1976).

3. R. R. Greene and C. W. Spofford, "Comparisons of NADC Measured Bottom Loss With BLUG Simulated Bottom Loss," SAI-84-138-WA (March 1983).

4. R. L. Dicus, private communication.

5. I. M. Besieris and W. E. Kohler, "Two-Frequency Radiative Transfer Equation for a Statistically Inhomogeneous and Anisotropic Medium," in Multiple Scattering Waves in Random Media, edited by P. L. Chow, W. E. Kohler, and G. C. Papanicolaou (North-Holland, Amsterdam, 1981).

6. G. S. Brown, "Backscattering from a Gaussian-Distributed Perfectly Conducting Rough Surface," IEEE Trans. AP-26, 472-482, 1978. See also "Correction to above," IEEE Trans. AP-28, 943-946, 1980.

REFERENCE B

MEASUREMENTS OF BASEMENT ROUGHNESS AND SEDIMENT THICKNESS STATISTICS IN PACIFIC ABYSSAL HILLS

Pre-publication, submitted to
Journal of Geophysical Research

Measurements of Basement Roughness and Sediment Thickness Statistics in Pacific Abyssal Hills

C. W. Spofford and E. S. Holmes

Science Applications International Corp.

F. N. Spiess

University of California

Short Title: Pacific Basement Roughness

Address List

C. W. Spofford

E. S. Holmes

Science Applications International Corp.

1710 Goodridge Drive

McLean, VA 22102

F. N. Spiess

Institute of Marine Resources

University of California

La Jolla, CA 92093

ABSTRACT

Deep Tow data from an abyssal-hill site in the Northeastern Pacific (north of Hawaii) have been analyzed to estimate the statistics of basement roughness and sediment thickness. Specifically, basement roughness spectra have been developed, tested for directionality and stationarity, and compared with Bell's results [1975] for a similar area but larger wavelengths. Distribution functions of basement height (detrended) and slope and sediment thickness are also presented.

Ocean bottom roughness is a quantity of interest to both the geophysical and acoustical communities. Roughness varies from large scale features which are essentially bathymetry to features whose scale lengths are so short that only statistical descriptions are appropriate. Geologists have found roughness a useful description of the ocean bottom. In addition, oceanographers have shown an interest in roughness

as a generator of open-ocean internal waves [Bell, 1975], and acousticians have seen roughness as a mechanism for scattering of bottom-incident sound waves [Berkson and Matthews, 1984].

In the abyssal hills of the North Pacific at acoustical frequencies from tens to thousands of hertz the bottom properties of most importance are the sediment thickness to the first major internal reflector and the roughness of that interface. The relatively small impedance contrast at the water-sediment interface produces low reflectivity compared to that caused by the large contrast at this strong reflector in this frequency regime. The high impedance contrast at this reflecting horizon (acoustic basement), together with its roughness, tends to scatter back into the water column a large amount of energy over relatively wide angles [Spofford, 1983; Diachok et al., 1984].

The acoustical properties of interest for this problem are the various wave speeds and attenuations, the impedance contrasts, the sediment thickness, and the scatter-controlling aspects of basement roughness. This paper is concerned with estimates of the last two properties for an

abyssal-hill environment representative of large regions of the North Pacific. The data used to address these issues were collected during a Deep Tow survey [Spiess and Lonsdale, 1982] of a manganese nodule site in the North Pacific known as MANOP Site R. The original goals of the expedition were to map the local variability of the extensive nodule coverage at this latitude using near-bottom side-looking sonar and photography, and to determine sites which would be appropriate for subsequent deployment of bottom landing vehicles to carry out experiments in the sediment. Site R was selected as typical of the extensive nodule-covered red clay region of the North Pacific. The total sediment column, as determined by seismic refraction stations within a few hundred miles, ranges from 300 to 500 m [S. M. Smith, SIO, personel communication]. The first major internal reflector, constituting the effective "basement" for the acoustic aspects considered here, lies at a depth of 30 to 50 m below the sea floor. The dense surficial manganese nodule coverage makes the sea floor itself the major reflector at frequencies above a few thousand hertz, and at 4 kHz there are two additional weak reflectors discernable above the effective acoustic basement [Spiess and Weydert, 1984].

Data from over 100 km of tracks crisscrossing a 200 sq km area were analyzed with the primary objective of describing the topographic roughness of the major internal reflector and a secondary objective of characterizing the thickness of the sediment overlying it.

Most data on seafloor roughness are collected with various instruments at (or very near) the ocean surface and have limited spatial resolution. Berkson and Matthews [1984] summarize data that typically resolve features with scale lengths of 200 to 2000 m. Only scale lengths greater than half the acoustical wavelength can contribute to the scattered field; hence most of the previous roughness data are not applicable to the basic scattering problem. However, when the roughness power spectrum appears to follow a simple power law, extrapolation to much shorter wavelengths might provide the necessary data.

The roughness issues that this analysis specifically addresses are:

(1) Power spectra at wavenumbers of acoustical interest

(2) Directionality of basement spectra

(3) Spatial stationarity

(4) Consistency with longer wavelength data (including the extrapolation issue)

(5) Height distributions

(6) Slope distributions.

In addition, distributions of sediment thickness have been computed.

The following sections describe, respectively, the measurement apparatus, the data processing and analysis, the results, and the conclusions regarding these issues.

MEASUREMENT APPARATUS

The Deep Tow Instrumentation System, originally deployed in 1962, has undergone a series of augmentations, allowing it to examine with increasing resolution and diversity the

properties of the sea floor. Typically Deep Tow (fish) is towed 10-100 m above the sea floor. A 12-kHz transponder net is deployed on the bottom allowing the tow-ship and the fish to determine their positions relative to the bottom with accuracies of 20 m and 2 m respectively.

The recordings of interest to this analysis are made using the 4-kHz seismic profiler [details may be found in Lonsdale, Tyce and Spiess, 1974]. Although this system is effectively omnidirectional, it is so close to the bottom that it has an effective resolution of a few meters for the roughness seen in this area.

The soundings are virtually continuous and produce a graphic-recorder depth chart for the fish and for all reflectors (in this case the water-sediment and sediment-basement interfaces) versus time. From the geometry reconstructed using the transponders, time is converted to position.

DATA PROCESSING AND ANALYSIS

Figure 1 illustrates the entire Deep Tow track at the Manop "R" site. The origin (0,0) of the local coordinate

system was 30°19.9'N, 157°50.9'W. The heavy dashed and solid portions of the track were digitized. The portions not digitized had poor trace quality or too many interruptions to be useful for spectral estimates. The portions digitized but not analyzed had poor-quality information on the fish depth. The numbering scheme corresponds to specific analysis comments which follow.

For data-processing purposes, the fish track segments were smooth enough that we assumed $h(r) = h(s)$ where r is a straight-line range, s is path length along the actual track, and h is depth. Probability density functions of slope and sediment thickness were computed using unfiltered data. Basement depth distributions were computed after detrending, effectively simulating a high-pass filter (Figure 2). Note that the sea floor depth profile appears, in a sense, to be a low-pass filtered version of the topography of the first major reflector.

In spectral analysis, the high-pass wavenumber corresponded to a wavelength approximately one-tenth the length of the track being processed. Low-pass wavenumbers ranged from .008 m^{-1} for Track 8 to .025 m^{-1} for Track 6. One-dimensional power spectral densities were computed using an

FFT from windowed, detrended data. The window consisted of a raised cosine applied to the first and last one-eighth of the points on each track. The spectrum of the window has a side-lobe rolloff ($P(K) \sim K^{-5.6}$) much steeper than the spectra of the data, and a narrower main lobe than a Hanning window. Transform size depended on track length. Range steps were approximately 3.5 meters, providing spectral estimates to a maximum wavenumber of about 1 m^{-1}.

Where tracks were long enough, averages of adjacent segments of a track were used to produce a smoothed spectrum. In these cases, a runs test was used to determine a minimum subtrack length so that adjacent subtracks were uncorrelated.

RESULTS

Track 8 (see Figures 1 and 2) was chosen to illustrate results from individual tracks. The power spectral density for this track (Figure 3) can be approximated by $P(K) \sim K^{-b}$, where P is the one-dimensional power spectral density, K is wavenumber and b characterizes the slope (on log axes) of the higher frequency portion of the spectrum. For Track

8, b=3.8. Probability density functions of detrended basement depth, one-dimensional basement slope, and sediment thickness are shown in Figure 4. The one-dimensional rms basement slope for this track is 4.8 degrees. A gaussian slope distribution would imply an equivalent two-dimensional rms slope of 6.8 degrees.

Table 1 summarizes, for all tracks, the one-dimensional slopes, rms roughnesses, and values of b. Values of b were nearly identical for all the tracks (Figure 5) whereas rms roughness and rms slope varied by almost a factor of 2 (Table 1). Clearly over this area these statistical measures are not constant, indicating some degree of non-stationarity of the random process $h(\underline{x})$ which might be relevant to acoustical scattering effects. Tracks 2a, 6a and 8a (see Figure 1) were used to test for directionality of basement properties. Figure 6 illustrates the corresponding power spectra. Within the limits imposed by the relatively small samples it is difficult to discern a significant directionality.

Assuming approximate statistical homogeneity over the area, an ensemble-average spectrum was computed (Figure 7). In this region it is clear from the individual and ensemble

spectra that in the wavenumber domain from 10^{-2} to 10^{0} m^{-1} the spectral slope steepens substantially. This is not an artifact of the data processing or the omni-directional nature of the transducer. (The slight decrease in slope near 10^{0} m^{-1} might be a sampling artifact, or it might represent the beginning of a new transition to fine-scale roughness.)

In Berkson and Matthews [1984] other abyssal-hill areas of the Pacific show power spectra with slopes, b, between 2.2 and 4.9 for wavenumbers of .003 to .03 m^{-1}. Bell [1975] reported a spectrum representative of over 8000 km of profiles from published surface-source data and data taken by Mudie using Deep Tow in a different abyssal-hill area. These data have been plotted in Figure 8 along with our ensemble spectrum. Both the slopes and spectral levels in the common regions are in excellent agreement. Figure 8 clearly illustrates the danger in extrapolating the shorter wavenumber spectra to the higher wavenumbers of acoustical interest using only the spectral slope of the short-wavenumber data. However, the spectra derived from Bell's data (from a wide-area average) and from the data of the present study (from a relatively small area) match closely in the wavenumber region of overlap (.006-.03 m^{-1}). This match

suggests that, for wavenumbers greater than .006 m^{-1}, the basement roughness spectrum may be relatively universal. The agreement also suggests that below this wavenumber the true basement roughness and bathymetry have comparable roughness.

Finally, Figure 9 displays ensemble distribution functions of basement height, basement slope, and sediment thickness. Overplotted on the histograms are Gaussian distributions with the same means and variances as the corresponding data. The tendency for all three Gaussian curves to be broader than the apparent distribution functions means that the tails of the histograms are driving the variance of the Gaussians. For slope and sediment thickness these differences are not too important. The clearly non-Gaussian height distribution can pose significant problems for acoustical scattering theories, nearly all of which assume a Gaussian distribution for $h(\underline{x})$.

SUMMARY AND CONCLUSIONS

Deep Tow data from an abyssal hill area of the Pacific north of Hawaii have been analyzed to provide statistics of basement roughness and sediment thickness. Detrended

basement roughness shows rms height variations of between 2 and 6.5 m depending on the specific track in the region surveyed. Basement rms slopes varied between 3.7 and 8.6 degrees with rougher basements tending to show larger slopes. The height distribution is distinctly non-Gaussian, suggesting significant consequences for bottom-bounce scattering theories. The slope distribution is more nearly Gaussian.

Basement roughness spectra for the wavenumber domain 10^{-2} to 10^{0} m^{-1} show a range of logarithmic slopes between -3.5 and -4.0. Little directionality was found in the power spectra for a set of three crossing tracks. In the wavenumber region of data overlap, there was significant agreement in both level and spectral slope (-2.5) between the ensemble-averaged power spectrum from the Deep Tow data and Bell's [1975] large-scale Pacific power spectrum. The present study extends the basement power-spectrum measurements upwards by two wavenumber decades. These results should be applicable to acoustical scattering problems for frequencies up to at least a few hundred hertz.

ACKNOWLEDGMENTS

The collection of the Deep Tow data was supported by the National Science Foundation and Sandia Laboratories. The authors would like to thank the officers and crew of R/V Thomas Washington for their support. The data were processed by M. Linzer at Scripps. The analysis of the data for basement and sediment thickness was supported by the Bottom Interaction Program of NORDA under Contract N00014-83-C-0303.

REFERENCES

Bell, T. H., Topographically generated internal waves in the open ocean, J. Geophys. Res., 80, 320-327, 1975.

Berkson, J. M., and Matthews, J. E., Statistical characterization of sea floor roughness, IEEE J. Ocean. Eng. OE-9, 48-52, 1984.

Diachok, O. I., Dicus, R. L., and Wales, S. C., Elements of a geoacoustic model of the upper crust, J. Acoust. Soc. Am., 75, 324-334, 1984.

Lonsdale, P. F., Tyce, R. C., and Spiess, F. N., Near-bottom acoustic observations of abyssal topography and reflectivity, in Physics of Sound in Sediments, L. Hampton, Ed., New York, Plenum, 293-317, 1974.

Spiess, F. N. and Lonsdale, P. F., Deep tow rise crest exploration techniques, Mar. Tech. Soc. Jour., 16 (3): 67-74, 1982.

REFERENCES (Continued)

Spiess, F. N. and Weydert, M., Cruise report: Rama leg 1, MANOP Sites C and R, SIO Ref. 84-8, 1 March 1984, 23 pp.

Spofford, C. W., Status of the bottom-loss problem relative to bottom-bounce coherence, in Stochastic Modeling Workshop, October 26-28, 1982, C. W. Spofford and J. M. Haynes, Eds., NAVSEA 24-1 - 24-32, 1983.

Tyce, R. C., Mayer, L. A., and Spiess, F. N., Near-bottom seismic profiling: high lateral variability, anomalous amplitudes, and estimates of attenuation, J. Acoust. Soc. Am., 68, 1391-1402, 1980.

Table 1. Track and ensemble summary statistics

		σ_h(m)	σ_{SLOPE}(degrees)	b:S~K^{-b}
INDIVIDUAL	1	6.53	6.28	3.7
TRACKS	2	2.87	3.83	3.5
	3	3.12	4.40	4.0
	4	3.86	5.03	3.6
	5	4.34	8.59	4.0
	6	2.34	4.86	4.0
	7	3.79	6.79	4.0
	8	4.14	4.80	3.8
SHORT	2a	2.06	3.69	4.0
INTERSECTING	6a	2.34	4.86	4.0
TRACKS	8a	3.55	5.9	4.0
AVERAGE		3.9	5.31	3.6

ENSEMBLE SEDIMENT	μ=36.5 m
THICKNESS	σ=6.25 m

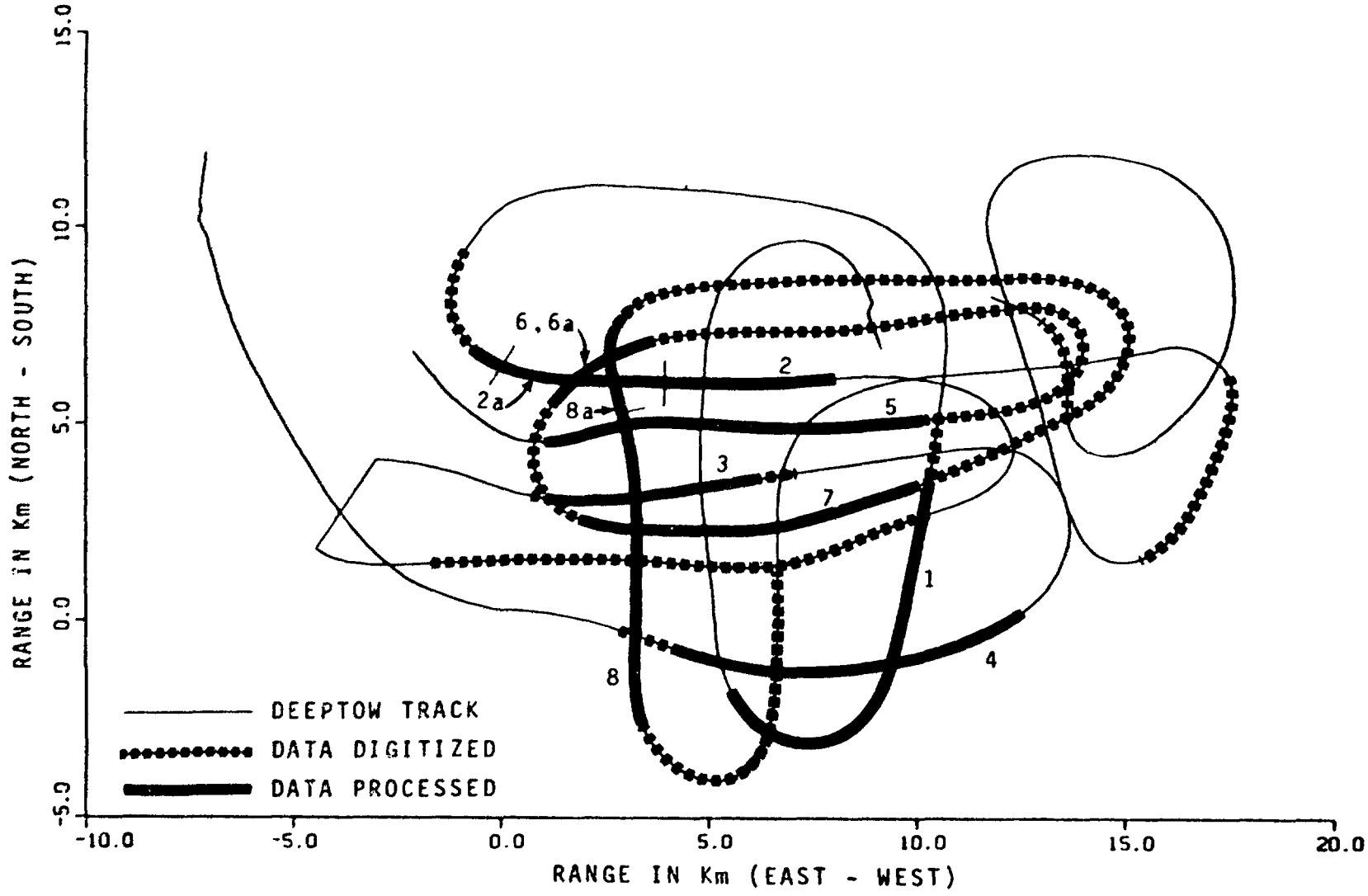

Fig. 1. Deep tow tracks in region.

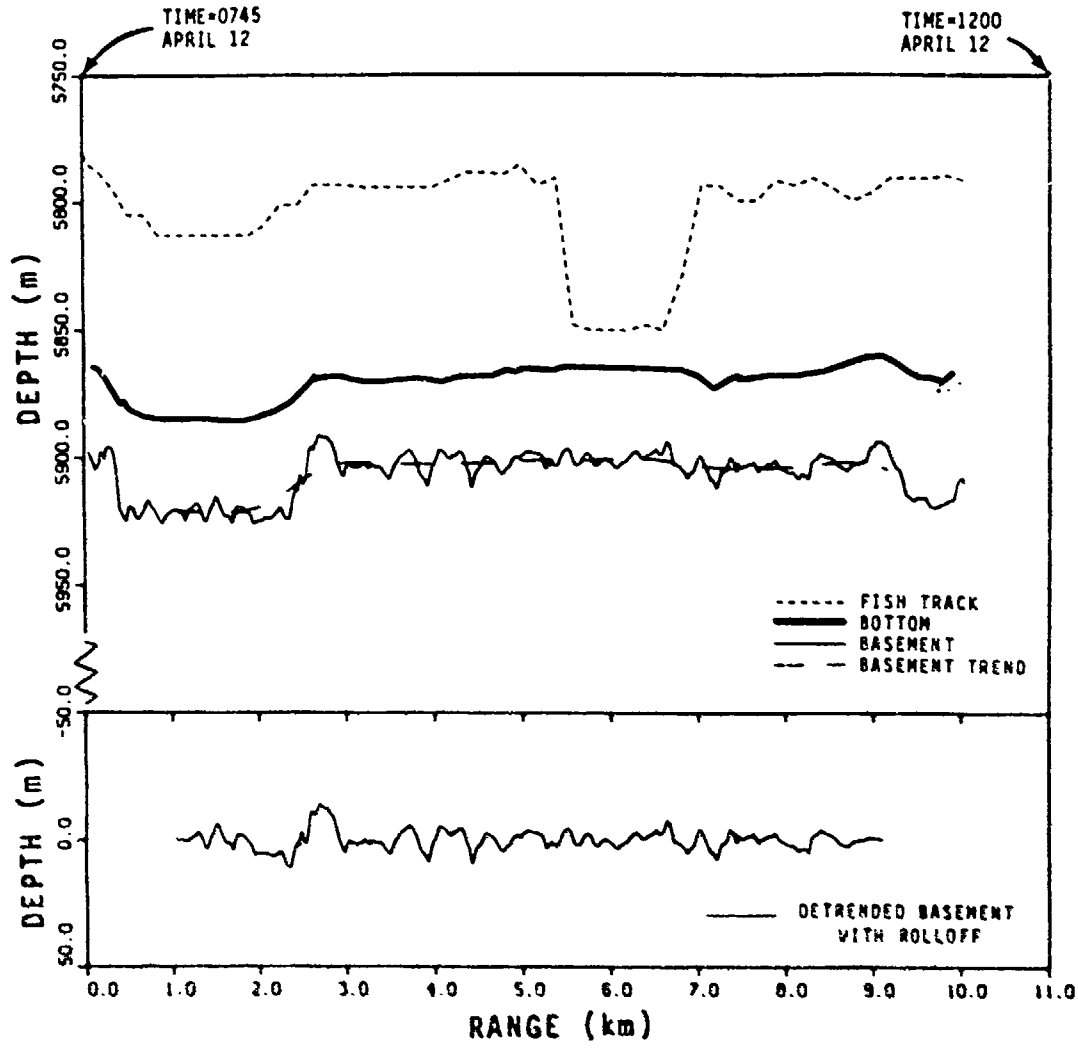

Fig. 2. Sample track-data for Track 8 of Figure 1.

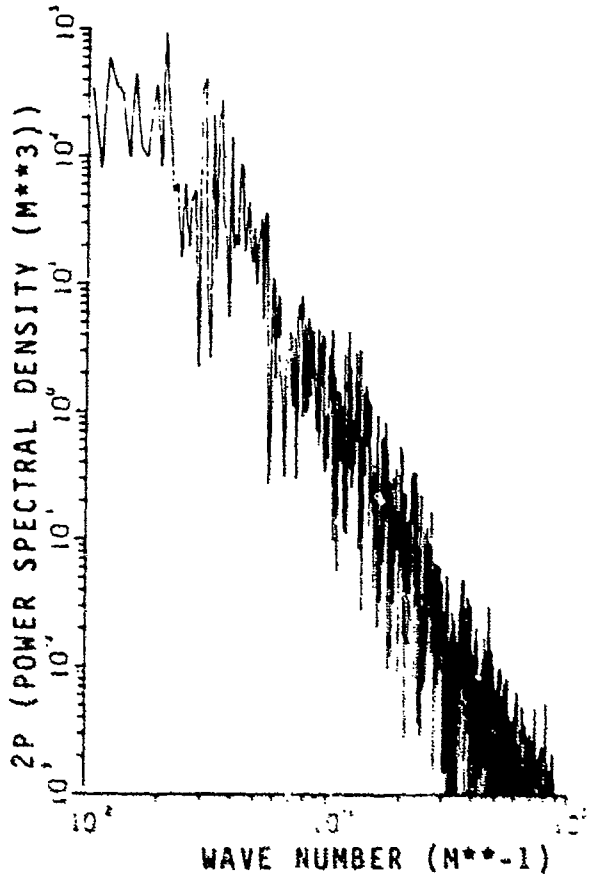

Fig. 3. Power spectral density of detrended basement depth for Track 8.

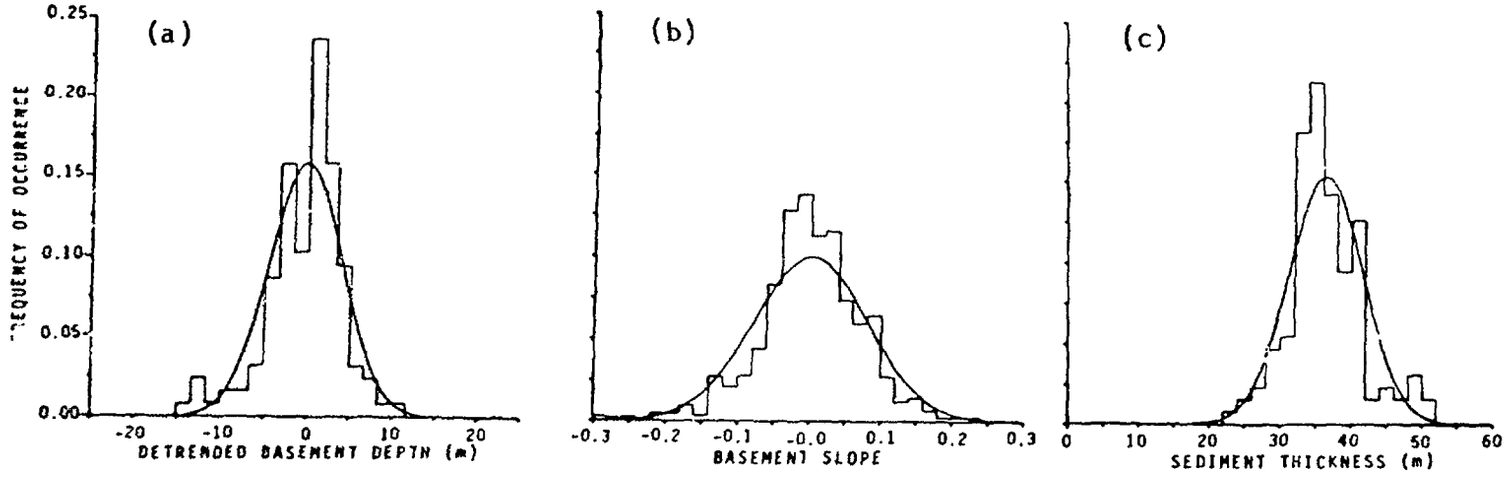

Fig. 4. Data histograms with corresponding Gaussian fits for Track 8: (a) detrended basement depth; (b) basement slopes; and (c) sediment thickness.

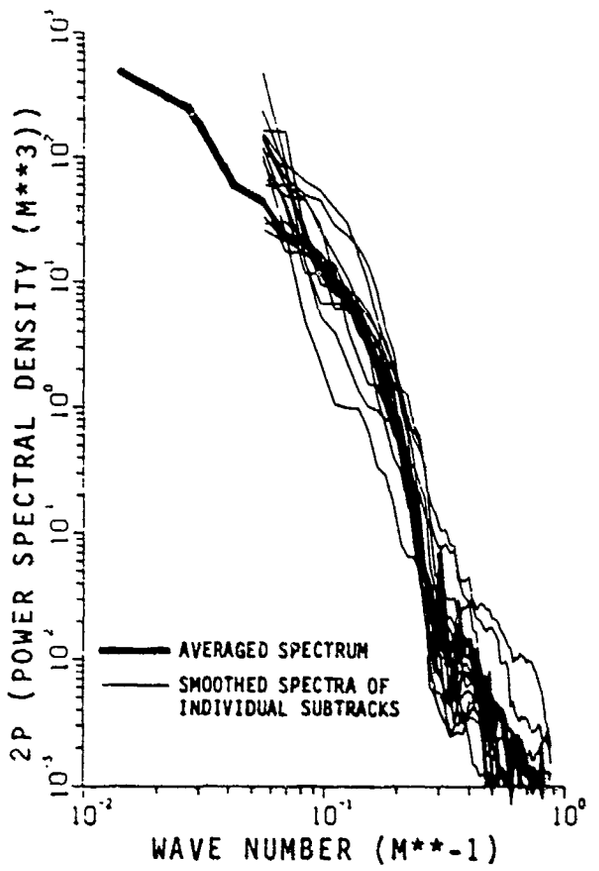

Fig. 5. Power spectral densities of detrended basement depth for all 8 tracks.

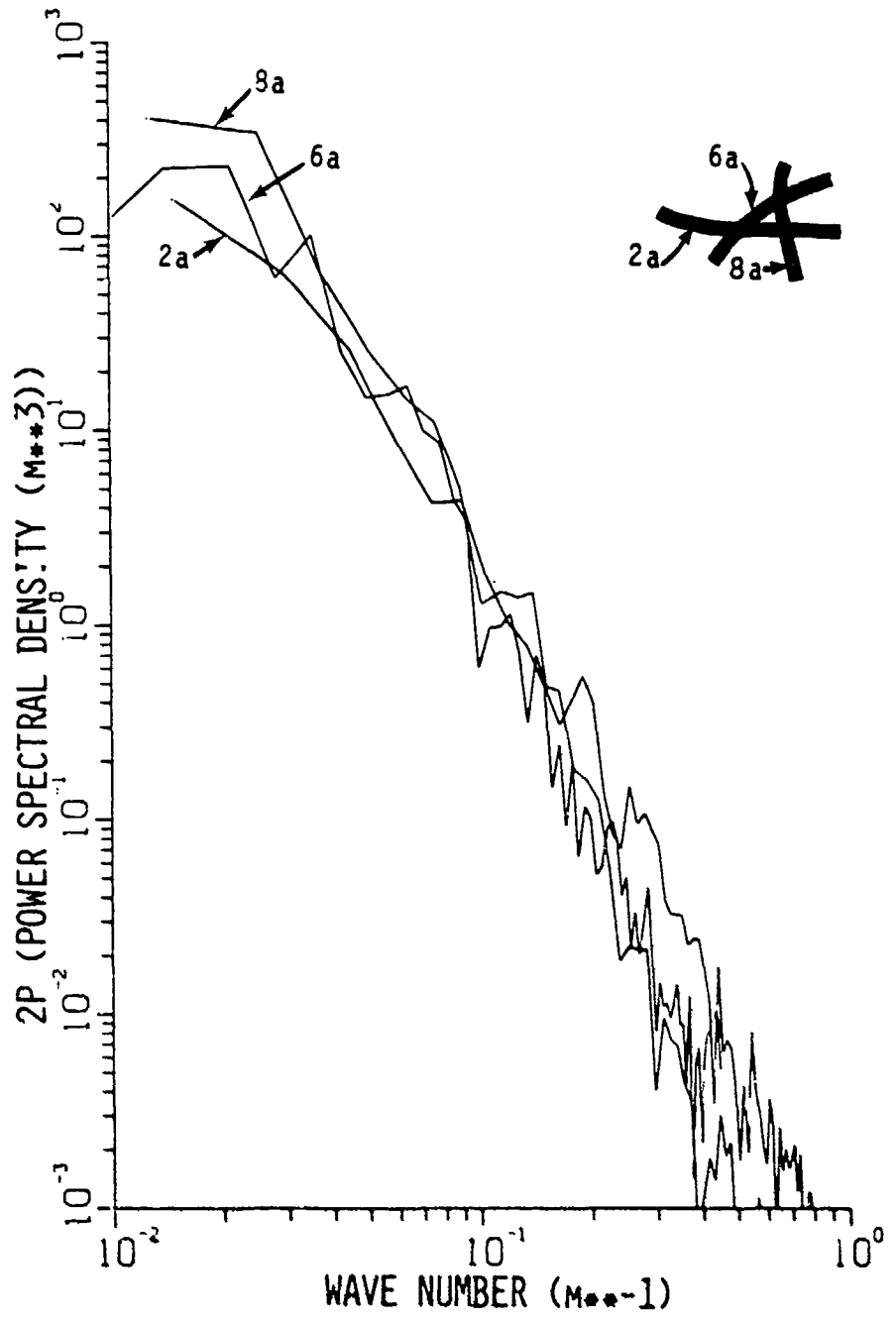

Fig. 6. Power spectral densities of crossing tracks to test potential directionality.

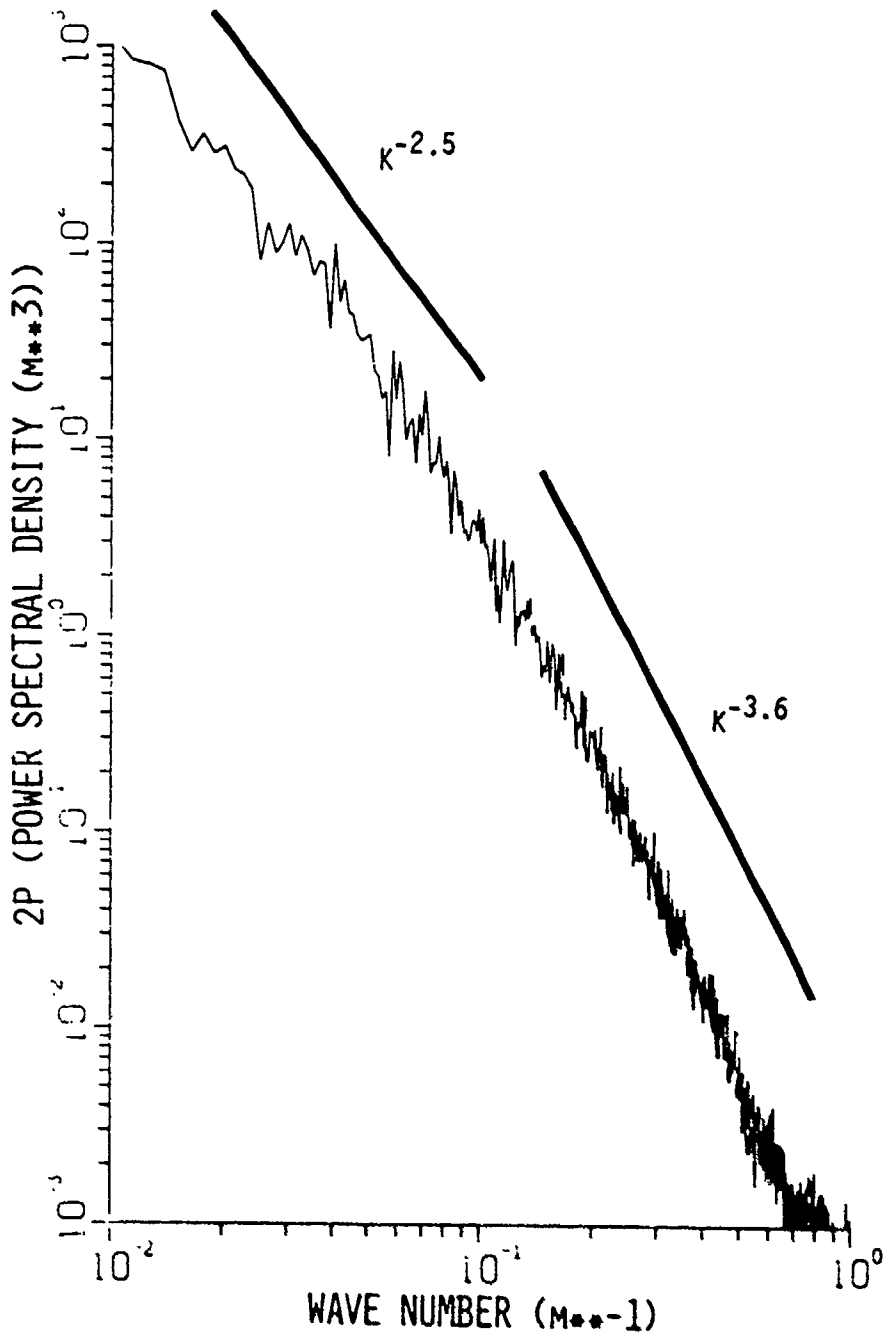

Fig. 7. Composite power spectral density averaged across all tracks.

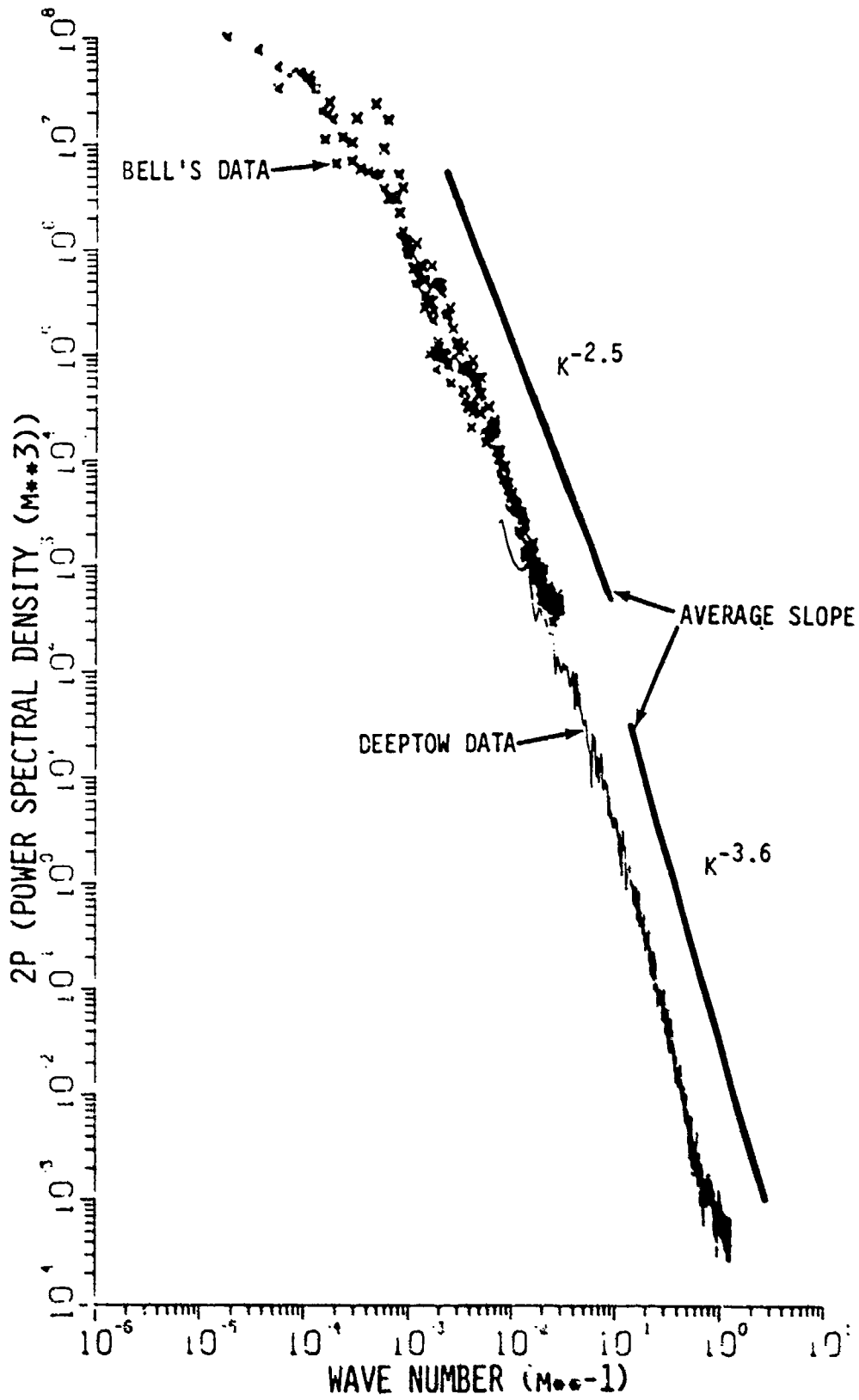

Fig. 8. Comparison of power spectral densities for low wave-numbers (Bell, 1975) and composite spectrum.

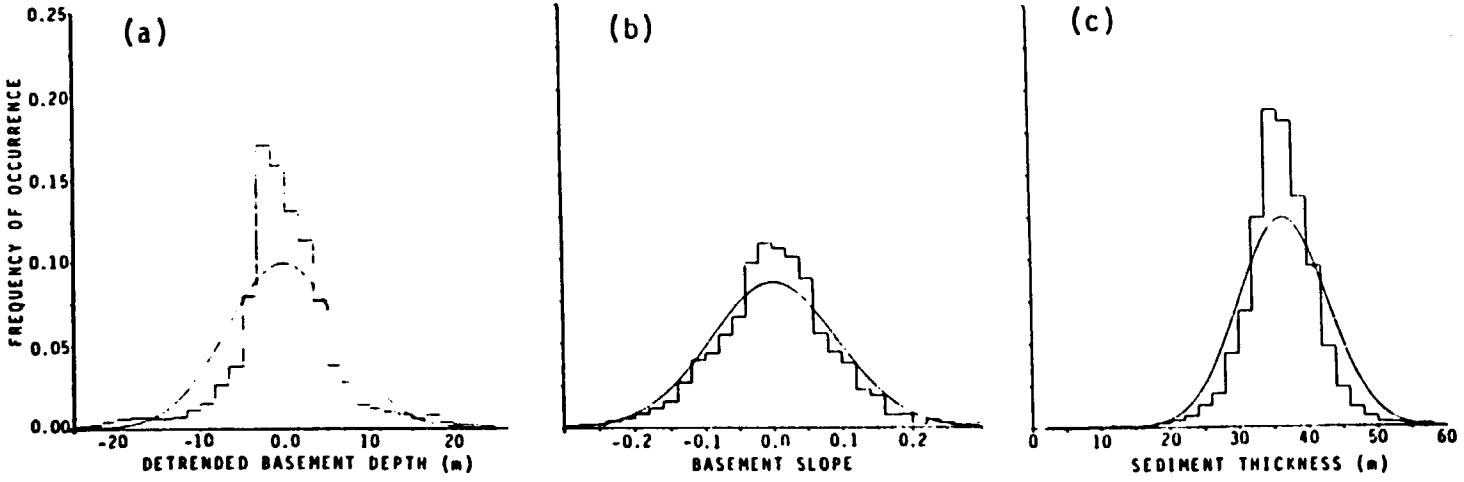

Fig. 9. Ensemble data histograms for all tracks with corresponding Gaussian fits; (a) detrended basement depth; (b) basement slope; and (c) sediment thickness.

DEPARTMENT OF THE NAVY
OFFICE OF NAVAL RESEARCH
875 NORTH RANDOLPH STREET
SUITE 1425
ARLINGTON VA 22203-1995

IN REPLY REFER TO:

5510/1
Ser 321OA/011/06
31 Jan 06

MEMORANDUM FOR DISTRIBUTION LIST

Subj: DECLASSIFICATION OF LONG RANGE ACOUSTIC PROPAGATION PROJECT (LRAPP) DOCUMENTS

Ref: (a) SECNAVINST 5510.36

Encl: (1) List of DECLASSIFIED LRAPP Documents

1. In accordance with reference (a), a declassification review has been conducted on a number of classified LRAPP documents.

2. The LRAPP documents listed in enclosure (1) have been downgraded to UNCLASSIFIED and have been approved for public release. These documents should be remarked as follows:

   Classification changed to UNCLASSIFIED by authority of the Chief of Naval Operations (N772) letter N772A/6U875630, 20 January 2006.

   DISTRIBUTION STATEMENT A: Approved for Public Release; Distribution is unlimited.

3. Questions may be directed to the undersigned on (703) 696-4619, DSN 426-4619.

BRIAN LINK
By direction

Subj: DECLASSIFICATION OF LONG RANGE ACOUSTIC PROPAGATION PROJECT (LRAPP) DOCUMENTS

DISTRIBUTION LIST:

NAVOCEANO (Code N121LC – Jaime Ratliff)
NRL Washington (Code 5596.3 – Mary Templeman)
PEO LMW Det San Diego (PMS 181)
DTIC-OCQ (Larry Downing)
ARL, U of Texas
Blue Sea Corporation (Dr.Roy Gaul)
ONR 32B (CAPT Paul Stewart)
ONR 321OA (Dr. Ellen Livingston)
APL, U of Washington
APL, Johns Hopkins University
ARL, Penn State University
MPL of Scripps Institution of Oceanography
WHOI
NAVSEA
NAVAIR
NUWC
SAIC

Declassified LRAPP Documents

Report Number	Personal Author	Title	Publication Source (Originator)	Pub. Date	Current Availability	Class.
Unavailable	Raysin, K. L.	COMPARISON OF OBSERVED AND PREDICTED AMBIENT NOISE IN THE NORTHEAST PACIFIC, WINTER 1980	Naval Postgraduate School	840601	ADB099796	U
Unavailable	Spofford, C. W.	FINAL REPORT ON CONTRACT N00014-83-C-0303	Science Applications International Corporation	850401	ADA155559	U